

**Probing Conformational Evolution and Associated Dynamics of Mg(N(SO<sub>2</sub>CF<sub>3</sub>)<sub>2</sub>)<sub>2</sub> ·**

**Dimethoxyethane Adduct Using Solid-state <sup>19</sup>F and <sup>1</sup>H NMR**

Ying Chen<sup>a</sup>, Nicholas R. Jaegers<sup>a</sup>, Kee Sung Han<sup>a</sup>, Hui Wang<sup>a</sup>, Robert P. Young<sup>a</sup>, Rajeev S. Assary<sup>b</sup>, Andrew Lipton<sup>a</sup>, Nancy M. Washton<sup>a</sup>, Jianzhi Hu<sup>a</sup>, Karl T. Mueller <sup>a\*</sup>, Vijayakumar Murugesan<sup>a\*</sup>

<sup>a</sup> The Joint Center for Energy Storage Research (JCESR), Pacific Northwest National Laboratory, Richland, WA 99352, USA

<sup>b</sup> The Joint Center for Energy Storage Research (JCESR), Argonne National Laboratory, Lemont, IL 60439, USA

\*To whom correspondence should be made

[Vijay@pnnl.gov](mailto:Vijay@pnnl.gov); (509) 371-6540

[Karl.Mueller@pnnl.gov](mailto:Karl.Mueller@pnnl.gov); (509) 371-6550.

## Abstract

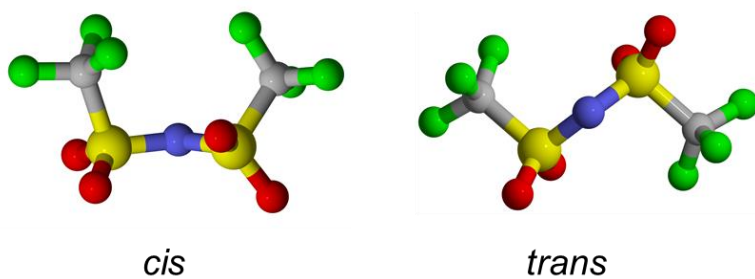
Bis(trifluoromethanesulfonimide) or TFSI is an important component in next-generation batteries and compounds containing TFSI have usually been characterized by vibrational spectroscopy (IR and Raman) and X-ray crystallography.  $^{19}\text{F}$  NMR is a similarly valuable diagnostic probe due to its high sensitivity to local chemical environments, as  $^{19}\text{F}$  has both a wide chemical shift range as well broad spans in the anisotropic component of chemical shift depending on local site symmetry and dynamics. Solution-state  $^{19}\text{F}$  NMR spectra of TFSI-containing solutions or ionic liquids produce a single resonance due to fast molecular motion, while solid-state  $^{19}\text{F}$  NMR spectra of TFSI containing salts yield broad (and often ambiguous) signals due to slow molecular motion. To capture detailed TFSI structural and dynamic changes using NMR, we explore the adduct of  $\text{Mg}(\text{TFSI})_2$  with dimethoxyethane (DME),  $\text{Mg}(\text{TFSI})_2\cdot\text{DME}$ . Within this system, TFSI molecular motion falls within the time scale of the NMR experiment, allowing for signature detection of TFSI states and conformers. Within the temperature range of -5 to 82 °C, we observe nine distinct TFSI sites in both crystalline and disordered regions, reflecting structural and dynamics changes of TFSI with temperature. The four distinguishable sites in the disordered region correspond to the four potential positions that can be occupied by the two  $\text{CF}_3$  groups of the same TFSI molecule. The exchange rate constants from site to site are calculated through variable-temperature  $^{19}\text{F}$  NMR and 2D exchange spectroscopy (EXSY) experiments, and activation enthalpies are obtained using Eyring's formulation. The flip rate of  $\text{CF}_3$  around the S-C bond is estimated as  $13.6 - 17.6 \text{ s}^{-1}$  at 8 °C with  $\Delta H^\ddagger = 19 - 24 \text{ kJ/mol}$ , but the rotation of the entire TFSI is  $4.8 \text{ s}^{-1}$  at 8 °C with a significantly greater  $\Delta H^\ddagger = 98 \pm 10 \text{ kJ/mol}$ . Furthermore, the slow conversion of *trans* to *cis* conformers at lower temperature ( $T \leq 1 \text{ }^\circ\text{C}$ ) in the crystalline region is monitored, with a conversion rate of  $1.9 \times 10^{-5} \text{ s}^{-1}$  at -5 °C. Density functional theory (DFT) based calculations were

performed to support further the assignment of experimental chemical shifts and the activation energy  $E_a = 21.1$  kJ/mol obtained for the *cis* to *trans* transition is consistent with experimental values. The combined set of  $^{19}\text{F}$  and  $^1\text{H}$  1D and 2D NMR methods demonstrated here can be further used for examining electrode-electrolyte interfaces where the time scales corresponding to the motions of TFSI and solvent molecules adsorbed at the interphase may enable detailed studies of interfacial structure and dynamics.

## Introduction

Bis(trifluoromethanesulfonimide) – TFSI - is a weakly coordinating anion widely used in ionic liquid (IL) solvents<sup>1, 2</sup> and is gaining greater attention as a promising electrolyte component in next-generation multivalent batteries.<sup>3-6</sup> For example, as the only readily ether-soluble simple Mg salt,  $\text{Mg}(\text{TFSI})_2$  -  $\text{Mg}(\text{N}(\text{SO}_2\text{CF}_3)_2)_2$  - has demonstrated remarkable electrochemical behaviors such as a wide electrochemical stability window and notable ion conductivity.<sup>6-11</sup> The enhanced solubility and electrochemical properties can be ascribed to the conformational flexibility of TFSI anions along with their extensive delocalized negative charge leading to a particularly weak coordinating power. Both theoretical and experimental studies have supported the existence of two conformers of C1 (*cis*) and C2 (*trans*) symmetry in TFSI-containing solutions and solids (Scheme 1),<sup>12, 13</sup> with the *trans* conformer 2-5 kJ/mol more stable in the gas phase, but the *cis* conformer preferred for coordinating multi-valent metal ions due to its larger dipole moment ( $\mu = 5.42$  D for C1 compared to 0.67 D for C2)<sup>12</sup>. In addition to the *cis* and *trans* conformers, TFSI anions can also establish mono- and bi-dentate coordinations involving sulfonyl oxygens and cation(s) as part of electrolyte solvation structures. These structural variations are complex and coupled closely to the thermodynamic landscape of ion diffusion pathways and exogenic forces (such as temperature and electric field), and therefore both structure and dynamics can play a critical role in overall battery

performance. For example, the solvate structure evolution near electrode-electrolyte interfaces during de- and re-solvation processes of cations in the presence of TFSI anions and solvent molecules will be critical in determining the rate of ion transfer between electrode and electrolyte. However, the absolute determination of the active solvate structure(s) enabling charge transfer remains elusive, necessitating ever more detailed molecular-level investigations of electrolyte constituents.



**Scheme 1.** Cis and trans conformers of TFSI. Atom color scheme: carbon = gray, nitrogen = blue, oxygen = red, fluorine = green, and sulfur = yellow.

Typical spectroscopic approaches such as IR and Raman studies exploit the specific vibrational modes of TFSI for analyzing conformational structures and provide specific spectral signatures for the two stable rotamers.<sup>6, 12-15</sup> However, the intrinsically weak signal intensity, potential fluorescence effect, and interfering peaks from other species may affect spectral interpretation. X-ray crystallography, especially single-crystal X-ray diffraction (SCXRD), directly detects TFSI geometries and has been used to determine the fraction of each conformer in several TFSI containing solids, but a well-defined crystal structure is required for the measurements and dynamics information is usually inaccessible.<sup>9, 16-20</sup> As one of the most sensitive NMR active nuclei, <sup>19</sup>F has proven to be a valuable probe in chemical, biological, and materials studies due to its wide chemical shift range and high sensitivity to its local chemical environment.<sup>21</sup> <sup>19</sup>F NMR

has been used in several TFSI containing solutions and ionic liquids providing useful information regarding the ion pairing of TFSI via self-diffusion coefficients measured by  $^{19}\text{F}$  pulsed-field gradient (PFG) NMR and about molecular rotational motions via NMR relaxation measurements.<sup>14, 22-25</sup> However, only a single  $^{19}\text{F}$  NMR resonance is observed due to the fast exchange rates ( $\geq \mu\text{s}$ ) between the conformers and associated structural variations within liquid electrolytes. As the solvent and/or anion exchange process within cation solvation structure can lead to motional averaging of NMR signal, NMR spectroscopic signatures and associated dynamics of different TFSI conformers within cation solvate structures can best be obtained if we limit (or “slow down”) molecular motion.

Nucleating crystals from saturated TFSI-based salt solution provide adduct structures containing TFSI, cations, and solvent molecules. This crystalline adduct structure represents a possible low energy solvation structure and offers a unique opportunity to study the conformational flexibility of TFSI in the presence of counter cations and solvent molecules with damped molecular motions that can readily be probed by NMR. In this work, we first present  $^{19}\text{F}$  magic angle spinning (MAS) NMR spectra on three TFSI-containing salts (LiTFSI, NaTFSI and Mg(TFSI)<sub>2</sub>), which show a general trend where signal from the *cis* conformer is shifted downfield from the *trans* conformer, but the broad signals resulting from slow molecular motion in salts prevent detailed structural and dynamic analysis. We then move to an adduct sample, Mg(TFSI)<sub>2</sub>·DME, where TFSI motion is slower than in pure liquids but faster than in pure salts, thereby enabling a detailed analysis of conformal structure and associated dynamics.  $^{19}\text{F}$  single-pulse 1D and 2D NOESY (nuclear Overhauser effect spectroscopy) and ROESY (rotating frame Overhauser effect spectroscopy) NMR studies of this adduct produce distinguishable signals for TFSI anions located in the ordered (crystalline) or disordered regions, adopting *cis* or *trans*

conformations. The conformational exchange rates between the conformers at varying temperatures are calculated from these 2D experiments. Additionally, DFT calculations of <sup>19</sup>F chemical shifts and the activation energy of *cis* to *trans* isomerization are consistent with the experimental values.

## Experimental Methods

**Sample preparation:** Salts of LiTFSI (Battery-grade, BASF), NaTFSI, and Mg(TFSI)<sub>2</sub> (99.5%, Solvionic) were dried for two days under vacuum at 180 °C prior to usage. The DME solvent (Battery-grade, Gotion) was further dried over activated 3Å molecular sieves in a glovebox until its moisture content was determined to be below 30 ppm using a Karl-Fisher Titrator (Metrohm). Mg(TFSI)<sub>2</sub> was dried for two days under vacuum at 180 °C until just before NMR measurements were made. Mg(TFSI)<sub>2</sub>·DME crystals were prepared based on a previously reported preparation method<sup>9</sup>: 3.65 g Mg(TFSI)<sub>2</sub> was dissolved and stirred in 4.5 g of DME at 80 °C for 24 h until no solids were visible in this solution. Subsequently, the hot solution was filtered through a 0.45 µm syringe filter, and the resulting filtrate was left undisturbed until it reached ambient temperature to separate out crystals.

**1D <sup>1</sup>H and <sup>19</sup>F NMR:** All samples were packed into 2.5 mm Bruker NMR rotors inside a glove box with a nitrogen atmosphere immediately before NMR measurement to minimize the influence of moisture. Dry nitrogen gas was used for MAS drive and bearing pressure thus further protecting the sample from moisture contact. Rotors allowed to remain at ambient laboratory atmosphere for even a few hours between measurements produced slightly different spectra, therefore, a fresh sample was prepared for each measurement. All experiments were repeated three times with freshly packed rotors. <sup>1</sup>H and <sup>19</sup>F magic angle spinning (MAS) NMR spectra were collected on a Bruker Avance III spectrometer with a field strength of 600 MHz (14.1 T) at a spinning speed of

24 kHz. The  $90^\circ$  pulse width was 3.2  $\mu$ s for  $^1\text{H}$ , and 3.3  $\mu$ s for  $^{19}\text{F}$ . The  $^1\text{H}$  and  $^{19}\text{F}$  spectra were obtained using single pulse excitation with 32 scans and a recycle delay of 20 s for quantitative comparison. For variable temperature MAS measurements, temperature calibrations were performed at various spinning speeds using lead nitrate ( $\text{Pb}(\text{NO}_3)_2$ ) powder as the sample temperature within a spinning rotor can be significantly different from the probe set temperature (supporting information).<sup>26, 27</sup> In variable temperature experiments, a series of spectra were measured once the temperature reading became stable and the results reported herein were for spectra that had reached equilibrium (no change was observed with time).  $^1\text{H}$  and  $^{19}\text{F}$  spin-lattice relaxation time ( $T_1$ ) measurements utilized the inversion-recovery ( $180^\circ - \tau_{\text{delay}} - 90^\circ - \text{acquisition}$ ) method, and spin-spin relaxation times ( $T_2$ ) were measured using the Carr-Purcell-Meiboom-Gill (CPMG) method ( $90^\circ - \tau_{\text{delay}} - [180^\circ - \tau_{\text{delay}}]_n - \text{acquisition}$ ) with a delay time  $\tau_{\text{delay}} = 83.33 \mu\text{s}$  ( $= 2/24 \text{ kHz}$ ), which was synchronized to the spinning speed of 24 kHz.

**2D  $^1\text{H}$  and  $^{19}\text{F}$  NMR:** 2D  $^{19}\text{F}$ - $^{19}\text{F}$  EXSY (NOESY) experiments were carried out using the “noesyph” pulse sequence included with Bruker’s Topspin® software with spectral width = 10 ppm (5647 Hz), number of increments = 128, number of scans = 8, and several mixing times (5, 10, 30, 50, 100, 300, and 500 ms) at 8 and 20 °C, but only two mixing times (30 and 50 ms) at other temperatures. 2D ROESY experiments used the pulse sequence “roesyph.2” in Topspin® software with the same parameters as those used for the NOESY experiment except that the number of scans was increased to 128 or 256 due to the lower sensitivity of the experiment, and the carrier frequency (o1p) was shifted 15 ppm downfield to minimize the TOCSY artifacts. 2D  $^1\text{H}$ - $^1\text{H}$  EXSY utilized similar parameters to the  $^{19}\text{F}$  experiments but with only one mixing time of 200 ms.

**Exchange rate constant calculation from 2D EXSY:** Due to the inherently much lower sensitivity in ROESY (via spin-spin relaxation) than NOESY (via spin-lattice relaxation), we calculated exchange rates using NOESY after first confirming that the cross peaks observed were indeed from chemical exchange and not the result of dipolar cross-relaxation via ROESY. In a 2D EXSY spectrum, 2D peak volume at row  $i$  and column  $j$  at a mixing time of  $t_m$  can be expressed as<sup>28, 29</sup>:

$$I_{ij}(t_m) = (e^{-\mathbf{R}t_m})_{ij} M_j^0$$

Here  $M_j^0$  is the magnetization of the nuclei at site  $j$  at equilibrium and  $\mathbf{R}$  is the rate-constant matrix with the values  $R_{ij} = -k_{ji}$ , the first-order exchange rate constant from site  $j$  to site  $i$ . Therefore, the rate-constant matrix can be calculated directly from the peak-volume matrix  $\mathbf{A}$ , with  $A_{ij} = I_{ij}(t_m)/M_j^0$ :

$$\mathbf{R} = -\frac{1}{t_m} \cdot \ln(\mathbf{A}) = -\frac{1}{t_m} \cdot \mathbf{U} \ln(\lambda) \mathbf{U}^{-1}$$

Here  $\mathbf{U}$  and  $\lambda$  are the eigenvectors and eigenvalues of  $\mathbf{A}$ .

In our case of four-site mutual exchange, with  $M_1^0 = M_2^0 = M_3^0 = M_4^0$ , we adopted a common treatment<sup>30</sup> to average out experimental error by replacing the cross peak volumes  $I_{ij}$  and  $I_{ji}$  by their average value  $(I_{ij} + I_{ji})/2$ . The rate constants were calculated at each mixing time, and the average value is reported.

The exchange rate constant,  $k$ , was obtained from 2D EXSY according to the Eyring formulation,<sup>43</sup>

44

$$\ln\left(\frac{k}{T}\right) = \ln\left(\frac{k_B}{h}\right) - \frac{\Delta H^\ddagger}{RT} + \frac{\Delta S^\ddagger}{R}$$

The enthalpy ( $\Delta H^\ddagger$ ) and the entropy ( $\Delta S^\ddagger$ ) of activation can be calculated from the slope and intercept of the Eyring plot of  $\ln(k/T)$  vs  $\ln(k_B/h)$ . Since we only have four reliable data points of rate constants vs. temperature, an unacceptable error can be associated with the intercept of the plot, so we only report  $\Delta H^\ddagger$  in Table 1.

### ***Computational Methods:***

DFT calculations were conducted with the Amsterdam Density Functional (ADF) software<sup>31-33</sup>. Initial cluster model geometries were obtained from previously reported crystal structures<sup>9</sup> and optimized using the generalized gradient approximation with Grimme's third generation dispersion-corrections with moderate BJ dampening applied to the Perdew-Burke-Ernzerhof functional [GGA: PBE-D3(BJ)].<sup>34, 35</sup> A Slater-type, all-electron, triple-  $\zeta$ , two-polarization function (TZ2P) was used as the basis set.<sup>36</sup> The numerical quality was set to Becke Excellent. NMR shielding tensors were calculated as implemented in ADF.<sup>37-39</sup> We employed 2,2,2-trifluoroethanol and trifluoroacetic acid as computational reference compounds with their experimental <sup>19</sup>F chemical shift at -77.8 and -76.55 ppm, respectively. The corresponding calculated <sup>19</sup>F chemical shifts in these compounds are -78.4 and -76.6 ppm; in reasonable agreement with the experimental observations.

## **Results and Discussion**

**TFSI conformational fingerprints using <sup>19</sup>F NMR chemical shift.** We began with three solid-state salts, LiTFSI, NaTFSI and Mg(TFSI)<sub>2</sub>, as their crystal structures with detailed TFSI conformal states were reported previously.<sup>16, 17, 19, 40</sup> As shown in Figure 1, clear differences in the chemical shift of the <sup>19</sup>F MAS NMR spectra are observed by changing cations, indicating the

presence of different TFSI conformational states due to the different cation size and ionic strength of the counter cation. For example, in anhydrous LiTFSI salt,<sup>17, 40</sup> the Li<sup>+</sup> is coordinated tetrahedrally to sulfonyl oxygen atoms from four different neighboring TFSI anions in *trans* conformational arrangements (see Figure 1a). This structural arrangement yields a nearly identical local environment at the terminal CF<sub>3</sub> groups thus giving rise to a sharp resonance at -79.1 ppm with a linewidth of 430 Hz. In the anhydrous NaTFSI salt,<sup>19</sup> the crystal structure has two ion pairs with two distinct Na<sup>+</sup> and TFSI in an asymmetric unit, in which both Na<sup>+</sup> cations have five primary coordinating oxygen atoms and two secondary coordinating atoms (one oxygen and one nitrogen), and both TFSI adopt a *cis* conformation. <sup>19</sup>F NMR of the NaTFSI salt (Figure 1b) shows three resonance at -76.21, -76.66, and -77.75 ppm, with the integrated ratios of 1: 1: 2, suggesting that the four CF<sub>3</sub> groups of the two TFSI experience slightly different local environments. Moving a step further from alkali to alkaline cation in anhydrous Mg(TFSI)<sub>2</sub>,<sup>16</sup> Mg<sup>2+</sup> engages in an octahedral manner to four TFSI with two TFSI providing two oxygen each and another two TFSI providing one oxygen each, so each TFSI in turn contacts two Mg<sup>2+</sup> with two oxygen from two different sulfur binding to one Mg<sup>2+</sup> and another oxygen binding to the second Mg<sup>2+</sup>. The uncoordinated oxygen in TFSI provides enough conformational freedom to adopt either the *cis* or *trans* isomer at the same positions within the crystal structure. Evidently, the Mg(TFSI)<sub>2</sub> crystal has 18% of *cis* and 82% of *trans* TFSI conformational arrangements, which is reflected as three <sup>19</sup>F MAS NMR resonances at -77.68, -78.98, and -79.84 ppm, with the integration ratio of 20: 5: 75 (see Figure 1c). The <sup>19</sup>F NMR chemical shift trends among these TFSI based salts reveals that the *cis* configuration exhibits downfield shifted signals relative to the *trans* configuration. Although local bonding environment can also dictate chemical shift, the general trend established for *cis* and *trans* configurations serves as an aid in the analysis of the conformational structure of

TFSI in different materials. Nevertheless, the local dynamics and associated conformational flexibility in these salt samples were not discernable by NMR owing to the much slower time scale of these processes resulting from stronger electrostatic interactions within these more rigid crystal structures.

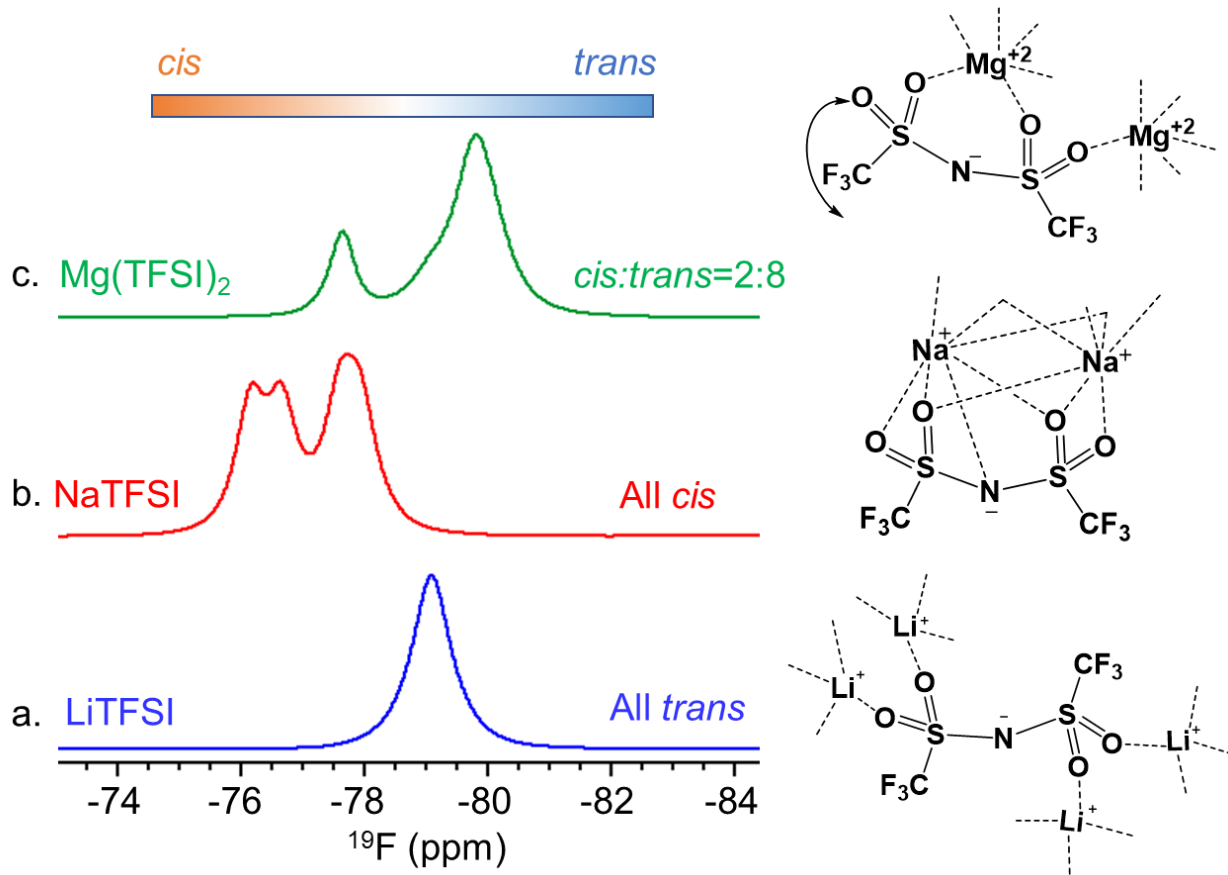


**Figure 1.**  $^{19}\text{F}$  MAS spectra of LiTFSI (blue), NaTFSI (red) and Mg(TFSI)<sub>2</sub> (green) collected at 20 °C with a spinning speed of 32 kHz.

Unlike the alkali and alkaline earth based TFSI salts, the DME based adduct structure ( $(\text{Mg}(\text{TFSI})_2\text{-DME})$ ) may offer enhanced conformational flexibility due to solvent molecules screening the electrostatic interaction between anions and cations. The crystal structure of this adduct material, reported by Salama *et. al.*<sup>9</sup>, showed that  $\text{Mg}^{2+}$  octahedrally coordinates with three

DME molecules in a bi-dentate formation whereas the TFSI anions are uncoordinated and approximately 4.5 Å away from Mg<sup>2+</sup> with highly disordered positions. This unique configuration could allow greater conformational flexibility for the TFSI molecules and offer an opportunity to establish a spectroscopic finger print and evaluation of the dynamics through consideration of chemical shift values, linewidth variations (motional narrowing), as well as 2D exchange experiments.

Figure 2 shows the <sup>19</sup>F MAS NMR spectrum of Mg(TFSI)<sub>2</sub>·DME obtained at a spinning of 24 kHz with a sample temperature of 8 °C. Deconvolution of the spectrum reveals six distinct resonances that can be grouped into two sets depending on the intensity and linewidth. The first set of resonances (represented by red lines) has four peaks centered at -76.96 (d1), -78.90 (d2), -79.70 (d3), and -81.10 ppm (d4), with identical intensity and linewidth (260 Hz). The next set constitutes two higher-intensity peaks located at -79.49 (O1) and -80.35 ppm (O2) with equal integrated area, albeit that O1 has a relatively narrower linewidth (108 Hz) than O2 (170 Hz). To correlate these peaks to respective sites of TFSI molecules within the adduct crystal structure, we performed 2-dimensional (2D) <sup>19</sup>F-<sup>19</sup>F NOESY and ROESY NMR measurements.

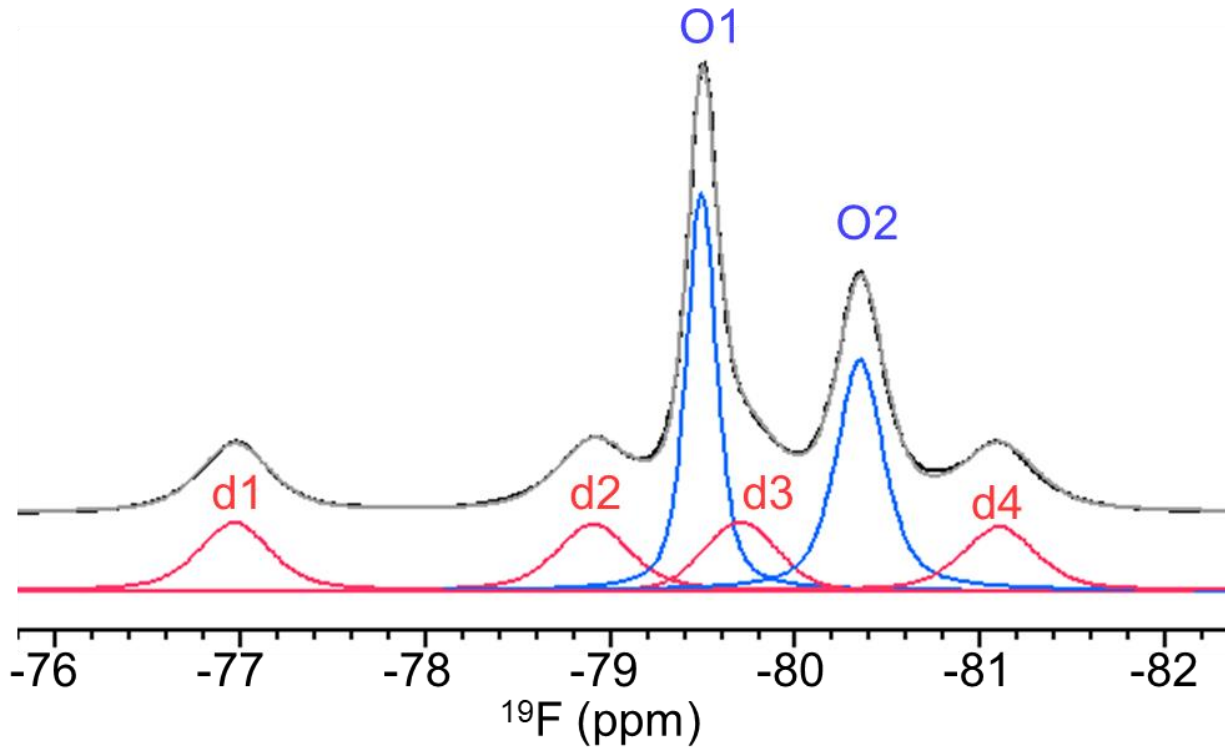


**Figure 2.**  $^{19}\text{F}$  MAS spectrum of  $\text{Mg}(\text{TFSI})_2\cdot\text{DME}$  collected at 8 °C with a spinning speed of 24 kHz. The black line is the experimental spectrum, red and blue lines represent the two sets of deconvolution peaks with the fractions  $f_{\text{d}1} = f_{\text{d}2} = f_{\text{d}3} = f_{\text{d}4}$  and  $f_{\text{O}1} = f_{\text{O}2}$ . The grey line is the sum of all deconvolution peaks.

Figure 3a shows  $^{19}\text{F}$ - $^{19}\text{F}$  2D NOESY spectrum of  $\text{Mg}(\text{TFSI})_2\cdot\text{DME}$  measured at room temperature. The NOESY correlation spectrum displays positive pure-phase cross peaks for both the first (d1, d2, d3, d4) and second (O1 and O2) set of resonances. These cross peaks could represent either dipolar coupling (due to closer proximity) or chemical exchanges between adjacent sites. To delineate between these two probable mechanisms, we performed  $^{19}\text{F}$ - $^{19}\text{F}$  2D ROESY measurements. In ROESY spectra, the cross peaks will register a negative intensity (opposite phase of the diagonal) if the underlying mechanism is the dipolar cross-relaxation through space.

Figure 3b shows the 2D ROESY spectrum where the cross peaks are positive for the first set of resonances (d1, d2, d3 and d4) and negative for the second set (O1 and O2). This indicates that the first set of four resonances (d1, d2, d3 and d4) are in chemical exchange with each other with distinguishable exchange rates, while the second set of resonances (O1 and O2) are being affected by dipolar coupling correlated through spin diffusion across closer proximity in space (typically  $<5$  Å). Note that although intra- and intermolecular F – F distances are usually  $> 4$  Å in Mg(TFSI)<sub>2</sub>·DME crystal structures,<sup>9</sup> the significant negative cross peak in ROESY may be the result from the strong spin diffusion effect, especially considering the bath of fluorine in the layered hydrophobic fluorous domain as reported in crystal structures of many TFSI containing salts.<sup>16-19, 41</sup>

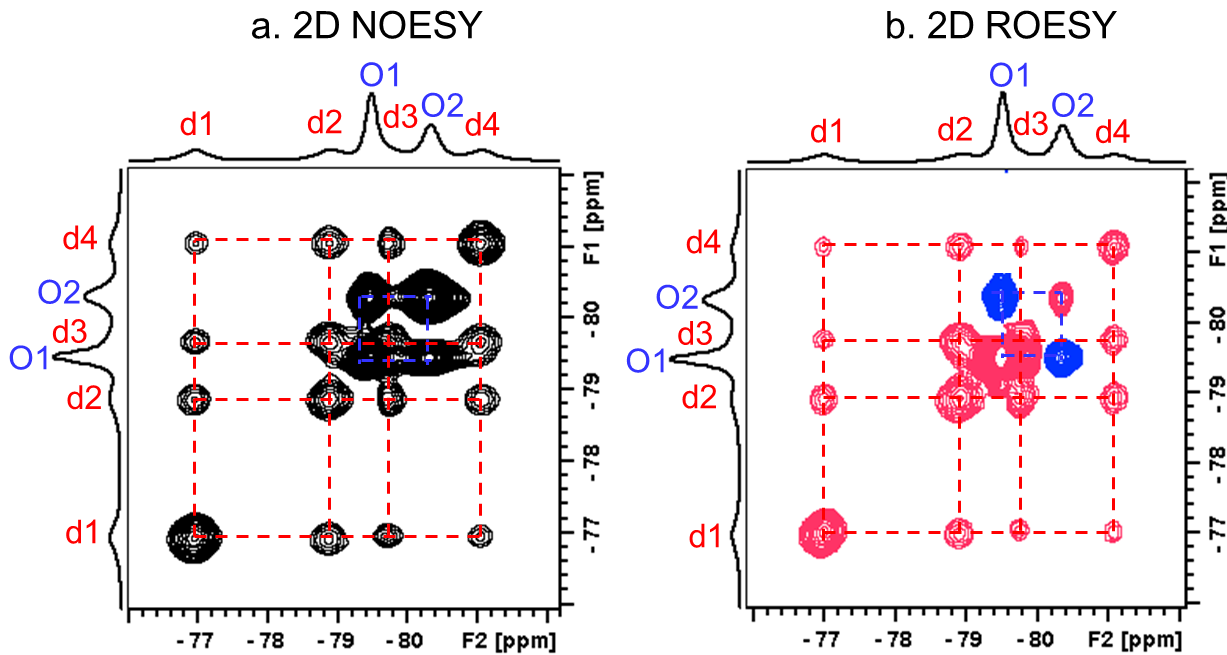


**Figure 3.**  $^{19}\text{F}$ - $^{19}\text{F}$  2D NOESY (a) and ROESY (b) spectra of Mg(TFSI)<sub>2</sub>·DME obtained at 8 °C with a spinning speed of 24 kHz and a mixing time of 30 ms. The experimental time for NOESY and ROESY measurement is 1.5 and 13.5 hours, respectively. In the 2D ROESY plot, the negative

cross peaks (between O1 and O2) are denoted with blue contours while the positive cross peaks (between d1, d2, d3 and d4) appear as red contours.

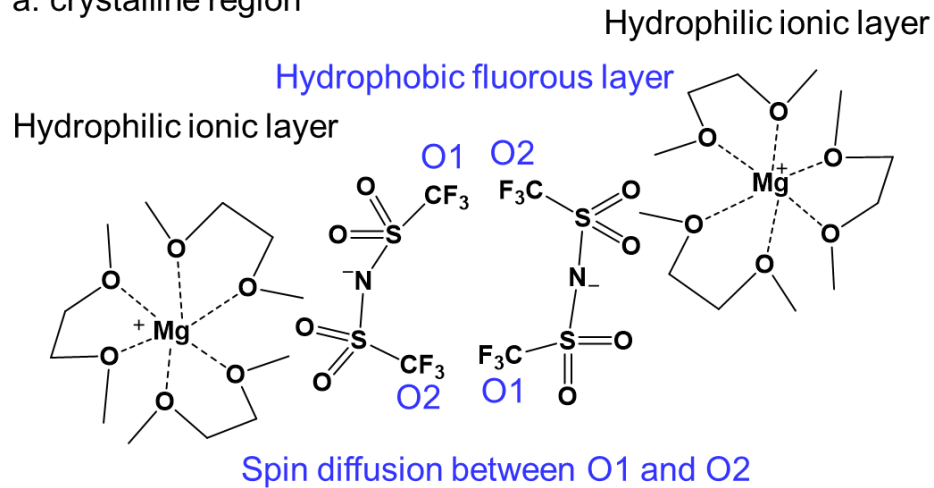
A reasonable model to explain these 1D and 2D NMR results together with previously reported single crystal structural data<sup>9</sup> is to categorize TFSI sites into two regimes, namely crystalline and disordered. In the crystalline region TFSI anions reside in the second coordinating shell of  $Mg^{2+}$ , whereas in disordered regions TFSI reside in third or fourth coordinating layers of  $Mg^{2+}$  that surround the crystalline region. A schematic illustration of these crystalline and disordered regions is shown in Scheme 2. The crystalline region has a hydrophobic fluorous layer where  $CF_3$  groups of adjacent TFSI molecules are packed closely leading to a dipolar coupled spin diffusion process, as indicated by the negative cross peaks in the ROESY spectra. Hence, we assign the resonances O1 and O2, with equal integration areas, to the two  $CF_3$  groups of one TFSI molecule within the hydrophobic fluorous layers of the crystalline region. The slightly larger linewidth of peak O2 may be explained by damped dynamics of this  $CF_3$  by its relatively closer proximity to  $[Mg(DME)_3]^{2+}$  than the  $CF_3$  of peak O1. On the other hand, the TFSI molecules in the disordered region reside further from the  $Mg^{2+}$  and hence have greater conformational flexibility leading to  $CF_3$  group exchange between different sites. Evidently, the four resonances with identical peak height and width, d1, d2, d3 and d4, correspond to the four sites that the two  $CF_3$  groups of a single TFSI molecule can occupy within the disordered region (Scheme 2b). The formation of the disordered region may be the result of 1) weak coordinating power of TFSI anions due to their conformational flexibility and highly delocalized charge, 2) weakened coordinating power of  $[Mg(DME)_3]^{2+}$  compared to  $Mg^{2+}$ , and 3) presence of remnant solvent DME from nucleation residing in the disordered region. The  $^1H$  NMR spectrum (Figure S3) confirms the presence of crystalline DME (well-defined  $^1H$  peaks at 4.20 and 3.90 ppm) and remnant DME (a broad peak

between 0 and 10 ppm). A certain amount of physically adsorbed DME may be left in the material during the drying process to produce crystals of  $\text{Mg}(\text{TFSI})_2\cdot\text{DME}$ . The supersaturated solution (3.65 g  $\text{Mg}(\text{TFSI})_2$  dissolved in 4.5 g DME) used to precipitate the crystal has a DME to  $\text{Mg}^{2+}$  ratio of 8, while DME to  $\text{Mg}^{2+}$  ratio is 3 for the crystalline region detected by SCXRD,<sup>9</sup> we have approximately two DME left in the disordered region, estimated from  $^1\text{H}$  NMR (Figure S3) and mass loss measurement. The fraction  $f_{\text{d}1+\text{d}2+\text{d}3+\text{d}4} : f_{\text{O}1+\text{O}2} = 0.55 : 0.45$  indicates that slightly more TFSI stays in the disordered region than the ordered region, which explains why SCXRD cannot accurately map TFSI positions. *TFSI anions in these two regions may exhibit similar properties as the solvent-separated ion pairs present in electrolytes and electrolyte-electrode interphases that play a key role in battery performance.*

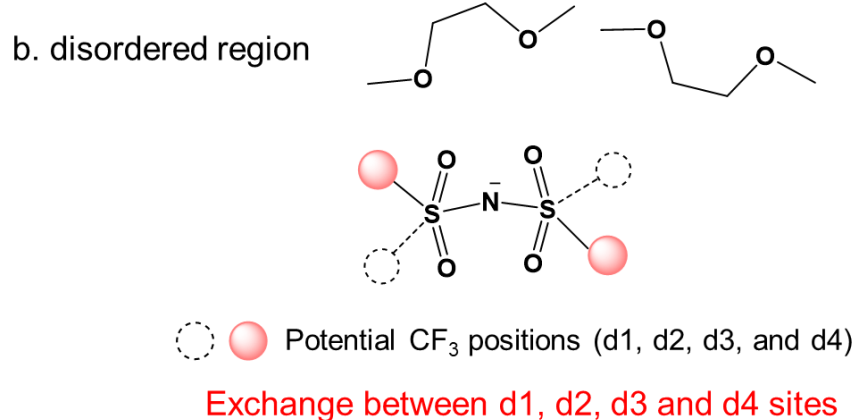
To further evaluate our model of correlating NMR resonances to TFSI conformational arrangements, we performed DFT based  $^{19}\text{F}$  chemical shift calculations. We begin with an isolated TFSI anion, where the *trans* configuration yields a single chemical shift value of -80.8 ppm whereas the *cis* configuration yields two distinct chemical shifts (-78.3 and -81.3 ppm) for the two  $\text{CF}_3$  groups. This is consistent with our previous observation (see Figure 1a) that the *cis* conformer appears downfield (by a few ppm) from the *trans* conformer. With this theoretically validated chemical shift trend, we performed large cluster DFT calculations of  $\text{Mg}(\text{DME})_3(\text{TFSI})_2(\text{DME})_n$  structures, which represents the disordered region. The choice of this cluster is based on a previously reported single crystal structure of the adduct material<sup>9</sup>. As shown in Figure S7,  $^{19}\text{F}$  chemical shifts of TFSI in the clusters are located between 76.6 and 81.0 ppm for clusters with  $n$  varying from 0 to 4. The significant variation in the calculated chemical shift with number of DME molecules in the secondary solvation shell is not surprising considering the oversimplification of a periodic crystalline structure to definitive molecular cluster models employed in our DFT

calculations. Nevertheless, the span of calculated chemical shifts ( $\sim 4.4$  ppm) of the clusters is consistent with the experimental value ( $81.10 - 76.96 = 4.14$  ppm, as shown in Figure 2), so it is reasonable to assume that the d1 to d4 sites are from TFSI located in the disordered region which resembles the  $\text{Mg}(\text{DME})_3(\text{TFSI})_2(\text{DME})_n$  clusters.

a. crystalline region



b. disordered region



**Scheme 2.** Schematic diagram of the two types of TFSI anions in  $\text{Mg}(\text{TFSI})_2\cdot\text{DME}$ . (a) Resonances O1 and O2 correlate to each other through spin diffusion in the hydrophobic fluorous layer of the crystalline region, and (b) resonances d1, d2, d3, and d4 exchange with each other by flipping of CF<sub>3</sub> group or rotation of the entire TFSI in the disordered region.

**TFSI conformational and dynamic changes.** Armed with spectroscopic signatures of different TFSI conformational structures within the adduct structure, we can now analyze the site-specific dynamics using variable temperature (from -5 °C to 82 °C) 1D and 2D NMR. A set of variable temperature 1D <sup>1</sup>H and <sup>19</sup>F NMR spectra are presented in Figure 4. As temperature increases, <sup>19</sup>F NMR reveals that the four resonances representing CF<sub>3</sub> sites within the disordered region (d1, d2, d3, and d4) undergo a coalescence process indicating thermally activated chemical exchange. At higher temperature (~52 °C) all four resonances coalesced to a broad resonance between -77 and -81 ppm and a small sharp resonance (d<sup≯</sup>) shifted towards high field (-79.25 ppm). The deconvolution analysis of this coalescence process is shown in the supplemental material (Figure S4). Similar to the observation in solid-state lithium ion conductors,<sup>42</sup> this composite of a narrow and a broad component in the NMR peak is caused by a distribution of CF<sub>3</sub> (TFSI) motions: the narrow component is from CF<sub>3</sub> with faster molecular motion, whereas the broad component is from CF<sub>3</sub> with slower motion. As the temperature increases further, the intensity of this sharp peak (d<sup≯</sup>) representing the disordered region increases at the cost of the broad peak as well as the broadening of resonances O1 and O2 from the ordered region. Meanwhile, <sup>1</sup>H NMR at high temperature ( $\geq$ 52 °C) also shows a new set of peaks located at 3.98 and 3.71 ppm, which are upfield shifted from the original peaks of solvate DME coordinated with Mg<sup>2+</sup> (i.e. [Mg(DME)<sub>3</sub>]<sup>2+</sup>). To further analyze these new peaks observed at higher temperatures, we performed <sup>19</sup>F-<sup>19</sup>F and <sup>1</sup>H-<sup>1</sup>H 2D NOESY measurements. The <sup>19</sup>F-<sup>19</sup>F NOESY spectrum (see Figure. 5a) indicates that the coalesced peak d<sup≯</sup> representing the disordered region does not correlate or exchange with O1 and O2 peaks of the ordered region. Similarly, the <sup>1</sup>H-<sup>1</sup>H NOESY spectrum (see Figure 5b) shows that the two new peaks are correlated with each other, suggesting that these two new <sup>1</sup>H signals are from DME molecules with slightly different chemical

environments than the solvated DME. It should be noted that the  $^1\text{H}$  NMR chemical shifts of neat DME are observed at 3.54 and 3.37 ppm, so the observed new peaks were potentially representing a new coordinating environment rather than representing “free” DME molecules. Additionally, the increase of the new  $^1\text{H}$  peaks is accompanied by the decrease of the signals from solvate DME, further suggesting structural evolution of solvated DME within the adduct structure. With the above combined information, we propose that when  $T \geq 52$   $^{\circ}\text{C}$ , some of the solvated DME molecules gain enough thermal energy to escape the first coordinating shell. This facilitates faster tumbling of TFSI in the disordered region, thus increasing the rate of chemical exchange between d1, d2, d3 and d4, yielding the coalesced new sharp peak d $'$ . In contrast, resonances O1 and O2 grow slightly narrower between 8  $^{\circ}\text{C}$  and 38  $^{\circ}\text{C}$  due to the increase of molecular motion of TFSI within the crystalline region. But the linewidths of O1 and O2 appear to be broadened at  $T \geq 52$   $^{\circ}\text{C}$ , probably due to the potential exchange that begins to happen between the two sites when the “escaping” solvate DME interacts with TFSI of the crystalline region. At 82  $^{\circ}\text{C}$ , the resonances O1 and O2 became closer to each other with significant line broadening due to further increase of the TFSI mobility as observed from the coalescing process of d1, d2, d3 and d4. A further increase in temperature may eventually access a state where molecular motion of all TFSI is on the NMR time scale leading to an exchange averaged single peak representing both the ordered and the disordered region that is similar to results from TFSI-containing solutions.

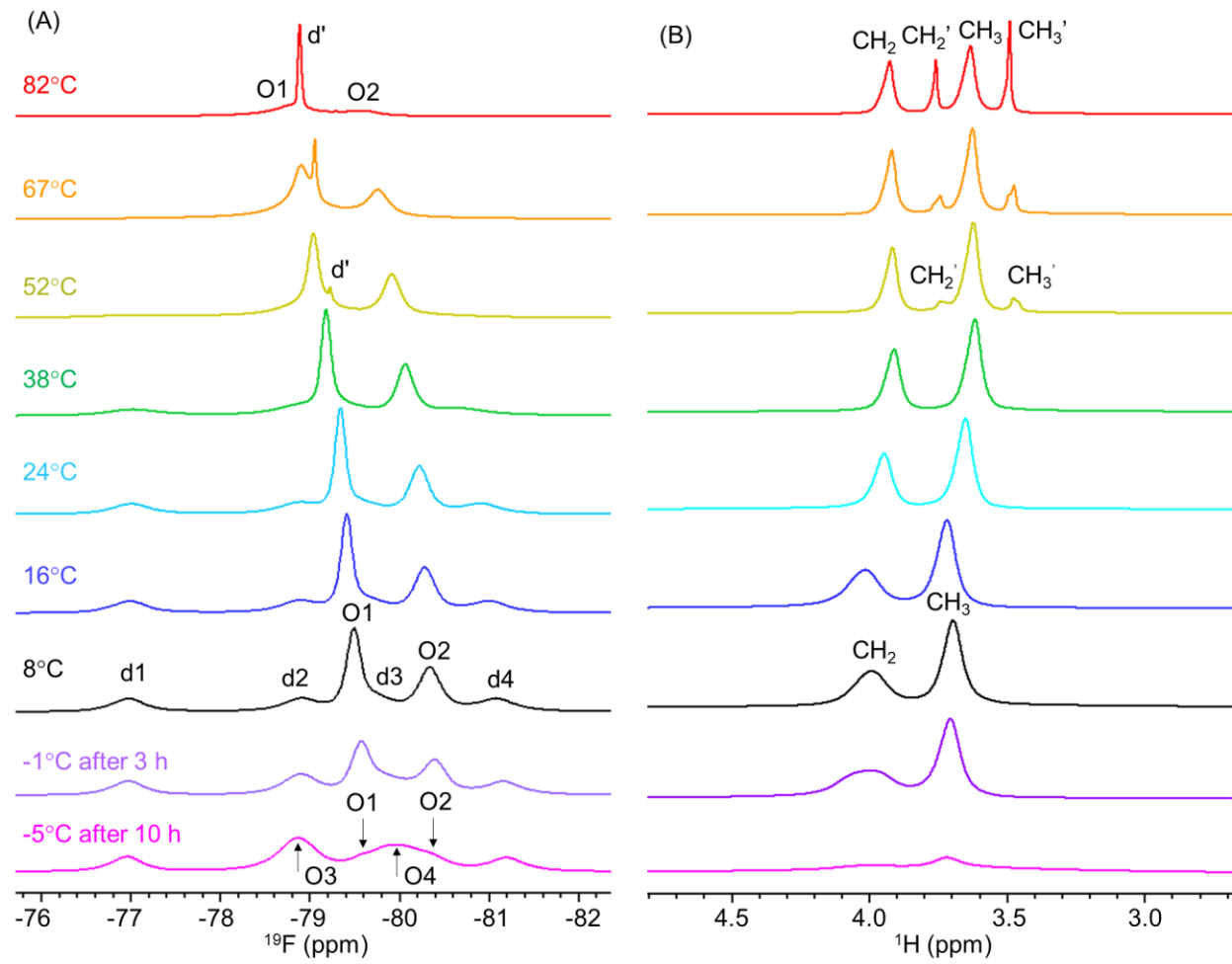


**Figure 4.**  $^{19}\text{F}$  and  $^1\text{H}$  MAS spectra of  $\text{Mg}(\text{TFSI})_2\text{-DME}$  from -5 °C to 82 °C acquired at equilibrium, with a spinning speed of 24 kHz.

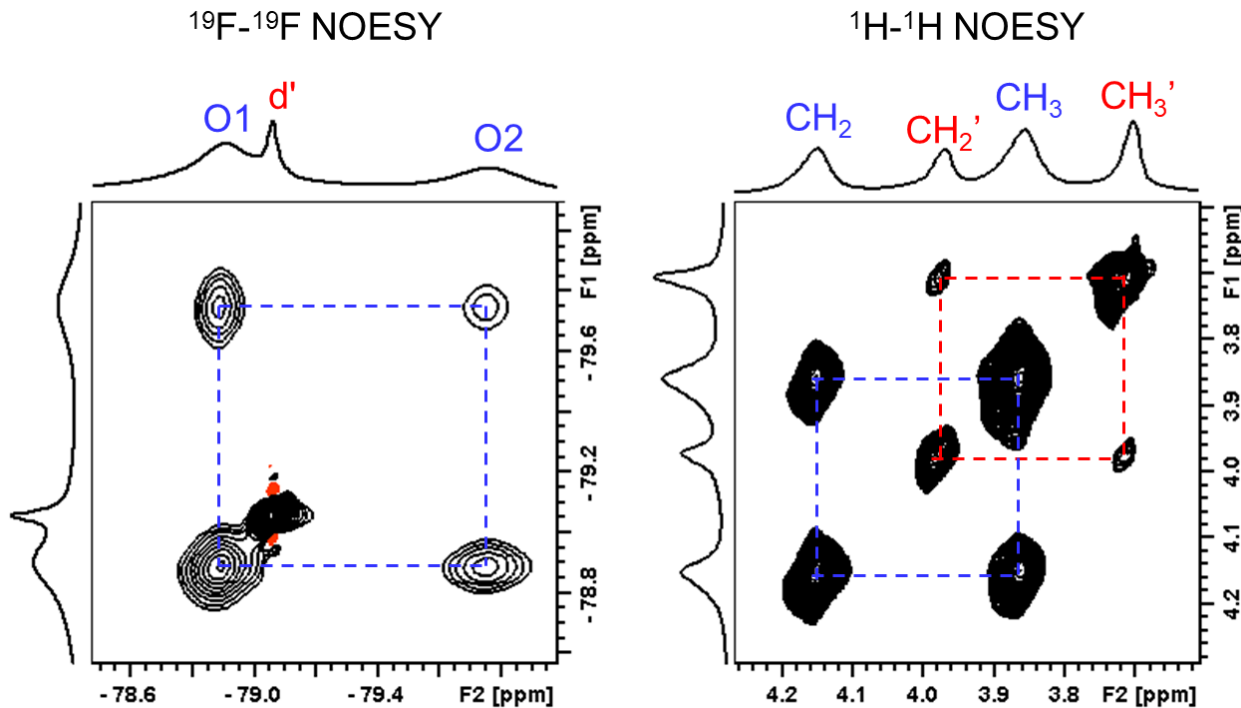


**Figure 5.**  $^{19}\text{F}$ - $^{19}\text{F}$  2D NOESY (left) and  $^1\text{H}$ - $^1\text{H}$  2D NOESY (right) spectra of  $\text{Mg}(\text{TFSI})_2\cdot\text{DME}$  obtained at  $67\text{ }^\circ\text{C}$  with a spinning speed of  $24\text{ kHz}$  and a mixing time of  $30\text{ ms}$  for  $^{19}\text{F}$ - $^{19}\text{F}$  NOESY and  $200\text{ ms}$  for  $^1\text{H}$ - $^1\text{H}$  NOESY.

In the low temperature regime ( $\leq 8\text{ }^\circ\text{C}$ ), the  $^{19}\text{F}$  NMR linewidth of resonances O1 and O2, representing TFSI molecules from the crystalline region, increases as evidenced by loss of signal height shown in Figure 4 (more detailed thermal and data analysis are reported in the supplemental section Figure S5). This line broadening leads to considerable signal overlap with d2 and d3 resonances. The peak deconvolution analysis based on a Gaussian/Lorentizan fitting method reveals the presence of new peaks (labelled as O3 and O4 in Figure 4) within this overlapped region. In order to validate the presence of these new peaks and to correlate with specific  $\text{CF}_3$  sites within the adduct structure, we performed  $^{19}\text{F}$ - $^{19}\text{F}$  2D NOESY experiments. The NOESY spectra measured at  $-5\text{ }^\circ\text{C}$  (see Figure 6), confirms the evolution of new resonances O3 and O4 located at  $-78.87$  and  $-79.93\text{ ppm}$ , which are  $0.72$  and  $0.48\text{ ppm}$  downfield shifted from O1 and O2

resonances of the crystalline region respectively. Similar to O1 and O2, O3 and O4 correlate with each other but not with any other peaks. Hence based on their chemical shift trend and dipolar relaxation induced cross peaks, we propose that O3 and O4 result from the two  $\text{CF}_3$  of the same TFSI with *cis* form at the second coordinating shell of the crystalline region, while O1 and O2 are from TFSI adopting the *trans* form. Similarly, the  $^1\text{H}$  NMR also shows a dramatic increase in linewidth of both  $\text{CH}_2$  and  $\text{CH}_3$  peaks with decreases in intensity, indicating that the conformational change of second-shell coordinating TFSI are correlated with the damped motion of coordinated DME within the crystalline region. It is intriguing to note the arising of new O3 and O4 peaks along with severely damped DME dynamics at lower temperature ( $\leq -5$  °C). Typically, at lower temperatures, restricted molecular motions would indicate preference for a more rigid crystal structure with higher coordinating power. For TFSI molecules, the relatively higher-coordinating *cis* conformer is preferred at lower temperature due to its greater dipole moment than the *trans* conformer ( $\mu = 5.42$  D in *cis* vs  $0.67$  D in *trans*)<sup>12</sup>. With increasing temperature, enhanced molecular motion of DME and TFSI favors a less rigid structure, therefore the *trans* conformer is preferred with only one side of  $\text{O}=\text{S}=\text{O}$  coordinating to  $[\text{Mg}(\text{DME})_3]^{2+}$  and the other side remaining more flexible. This conversion of *trans* to *cis* is a slow process with a reaction rate of  $\sim 2 \times 10^{-5}$  s<sup>-1</sup> calculated from the change of  $^{19}\text{F}$  NMR spectra with time at -5 °C.

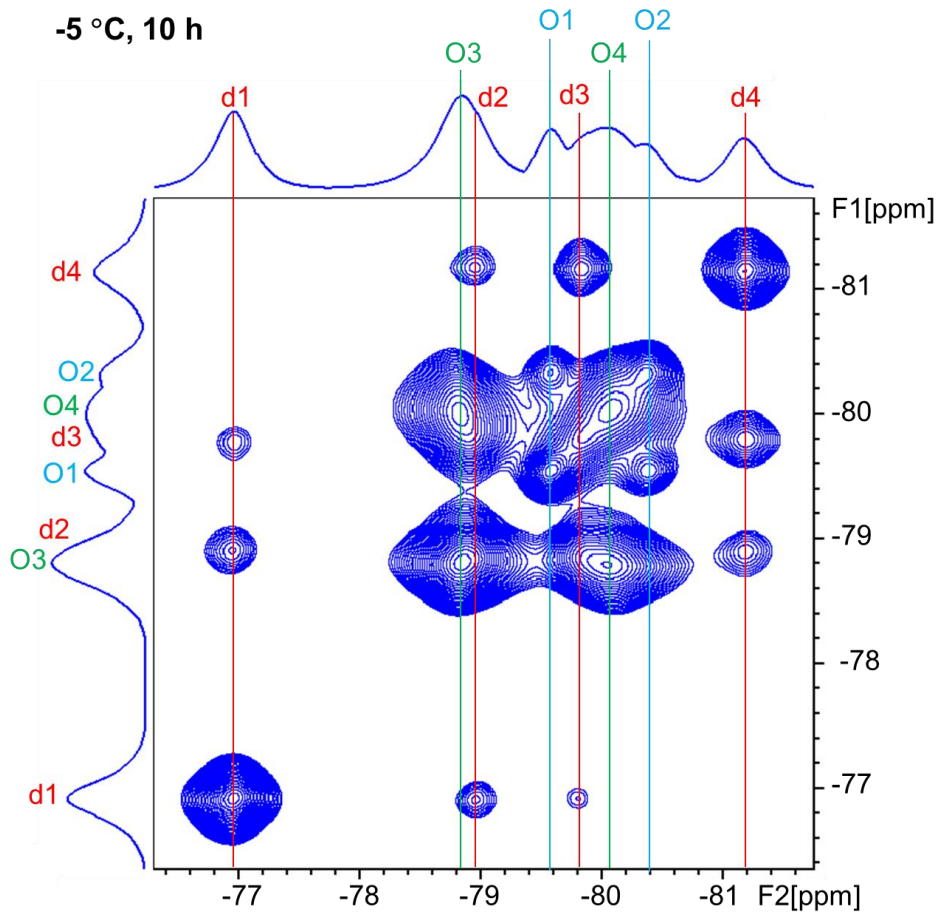
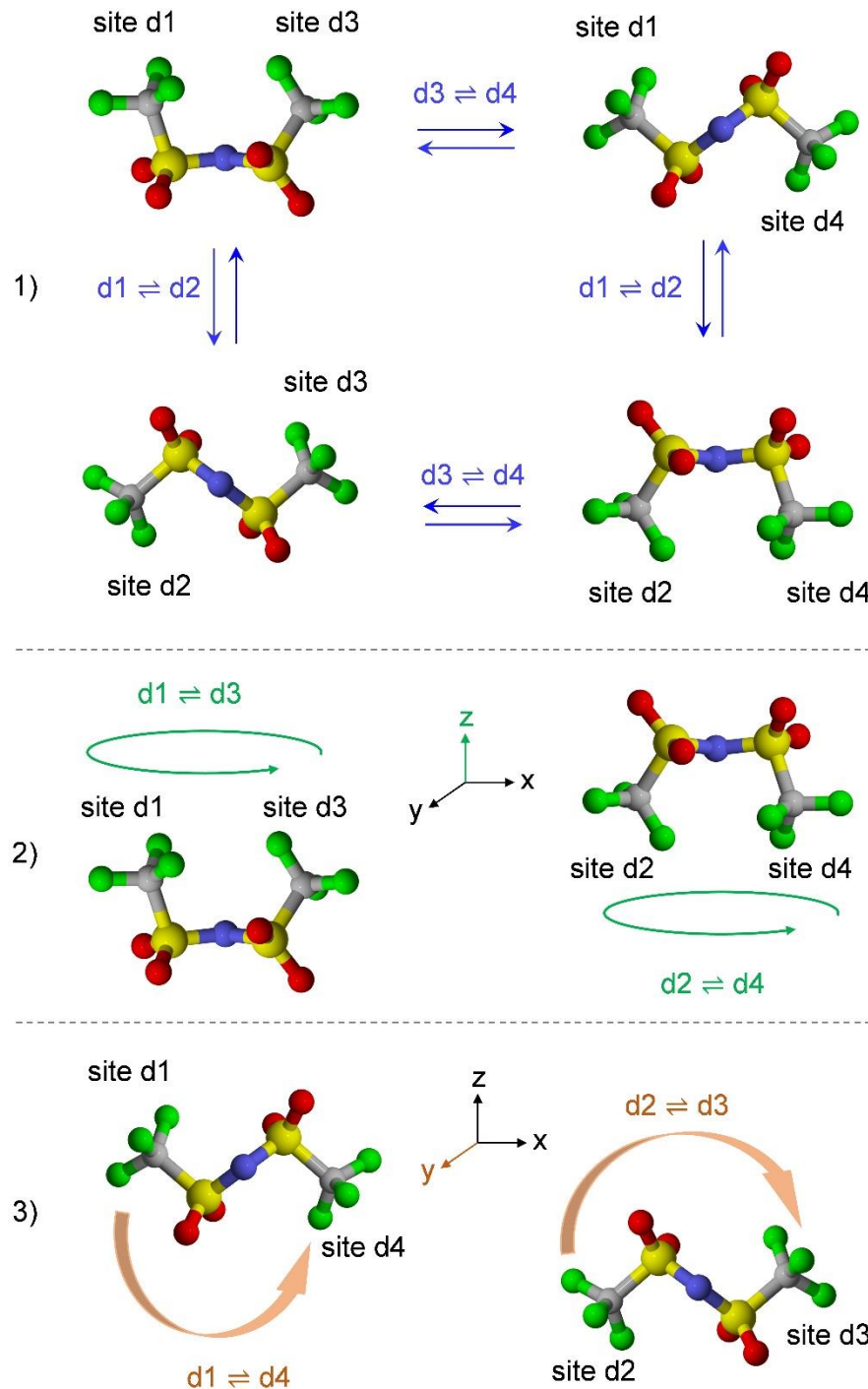


**Figure 6.**  $^{19}\text{F}$ - $^{19}\text{F}$  2D NOESY spectrum of freshly prepared  $\text{Mg}(\text{TFSI})_2\text{-DME}$  obtained at  $-5\text{ }^\circ\text{C}$  and equilibrated for 10 hours. The MAS spinning speed is 24 kHz and the mixing time is 30 ms.

**Thermodynamics and kinetics of TFSI conformational flexibility:** Since NMR detects site specific molecular motion directly, we can monitor the temperature dependent chemical and conformational exchange process within this complex adduct structure. As a first step, we calculated the exchange rate constants in the low temperature region (from 16 to  $-5\text{ }^\circ\text{C}$ ) between four sites d1, d2, d3, and d4 from 2D exchange spectroscopy (EXSY) (see experimental methods section for details). Although all exchanges between d1, d2, d3, and d4 are mutual, the rate

constants are significantly different, as shown in Table 1. When  $T \leq 8$  °C, the general trend is that  $k_{d1 \rightleftharpoons d2} > k_{d1 \rightleftharpoons d3} > k_{d1 \rightleftharpoons d4}$ ,  $k_{d3 \rightleftharpoons d4} > k_{d2 \rightleftharpoons d4} > k_{d2 \rightleftharpoons d3}$ . The fastest exchanges  $d1 \rightleftharpoons d2$  and  $d3 \rightleftharpoons d4$  may correspond to the flip of a  $\text{CF}_3$  group around the S-C bond, therefore  $d1$  and  $d2$  are attributed to the two sites that can be occupied by one  $\text{CF}_3$  group of TFSI in the disordered region, and  $d3$  and  $d4$  to the other  $\text{CF}_3$  group of the same TFSI (see Scheme 3). The slowest exchange  $d1 \rightleftharpoons d4$  happens between the two sites with largest chemical shift difference (4.14 ppm at 8 °C) indicating the exchange reflects the greatest change in the local chemical environment; hence we assign  $d1$  and  $d4$  to the opposite sides of S-N-S, and  $d1 \rightleftharpoons d4$  can only be realized by rotation of the entire TFSI anion by 180°. The potential chemical exchange processes between the four sites are summarized in Scheme 3: 1) rotation of S-C bond – flipping of  $\text{CF}_3$  group ( $d1 \rightleftharpoons d2$ ,  $d3 \rightleftharpoons d4$ ), 2) rotation of S-N-S bond along the z-axis that is within the S-N-S plane ( $d1 \rightleftharpoons d3$  and  $d2 \rightleftharpoons d4$ ), and 3) rotation of S-N-S bond along the y-axis that is normal to the plane ( $d1 \rightleftharpoons d4$  and  $d2 \rightleftharpoons d3$ ).



**Scheme 3.** Potential conformational exchange routes of TFSI in the disordered region.

Despite significantly different exchange rates, the activation enthalpy for TFSI conformational flexibility within the disordered region is comparable for  $d1 \rightleftharpoons d2$ ,  $d1 \rightleftharpoons d3$ ,  $d2 \rightleftharpoons d3$ ,  $d2 \rightleftharpoons d4$ , and  $d3 \rightleftharpoons d4$ . For example, the highest activation enthalpy of  $\Delta H_{d1 \rightleftharpoons d3}^\ddagger = 24 \pm 3$  kJ/mol and lowest enthalpy of  $\Delta H_{d3 \rightleftharpoons d4}^\ddagger = 19 \pm 3$  kJ/mol are observed for TFSI conformal exchange processes, suggesting that the transition between *trans* and *cis* conformers through flipping of a  $\text{CF}_3$  group around a S-C bond requires an activation energy of  $\sim 20$  kJ/mol in the low temperature regime. The exchange between  $d1$  and  $d4$  is the slowest at  $T \leq 8$  °C but becomes fastest when  $T \geq 16$  °C, yielding a dramatically greater activation energy  $\Delta H_{d1 \rightleftharpoons d4}^\ddagger = 98 \pm 10$  kJ/mol compared to other exchanges. This may be explained by the fact that this exchange demands the rotation of the entire TFSI and the interactions (electrostatic, dipolar and Van der Waals) between TFSI and its local environment including DME, other TFSI and  $\text{Mg}(\text{DME}_3)^{2+}$  are particularly not favorable for this exchange.

**Table 1.** Mutual exchange rate constants of  $d_1 \rightleftharpoons d_2$ ,  $d_1 \rightleftharpoons d_3$ ,  $d_1 \rightleftharpoons d_4$ ,  $d_2 \rightleftharpoons d_3$ ,  $d_2 \rightleftharpoons d_4$ , and  $d_3 \rightleftharpoons d_4$  calculated from 2D EXSY, and activation enthalpy  $\Delta H^\ddagger$  estimated using Eyring plot.

T (°C)\(k(s^{-1})\)	$k_{d_1 \rightleftharpoons d_2}$	$k_{d_1 \rightleftharpoons d_3}$	$k_{d_1 \rightleftharpoons d_4}$	$k_{d_2 \rightleftharpoons d_3}$	$k_{d_2 \rightleftharpoons d_4}$	$k_{d_3 \rightleftharpoons d_4}$
-5	7.6	3.1	0.7	6.4	7.8	10.4
1	10.4	4.5	2.0	8.4	11.5	13.0
8	13.6	5.6	4.8	9.5	12.1	17.6
16	16	7.5	19.2	15.0	17.8	19.7
$\Delta H^\ddagger$ (kJ/mol)	$21 \pm 3$	$24 \pm 3$	$98 \pm 10$	$23 \pm 3$	$21 \pm 3$	$19 \pm 3$

To further evaluate the energy requirements for the *cis* to *trans* conformational transition process for the TFSI anion, we calculated the activation energy by performing a pseudo rotation of TFSI with the dihedral angle  $\phi(\text{S}-\text{N}-\text{S}-\text{C})$  varying from  $-90^\circ$  to  $90^\circ$ , as shown in Figure 7. The activation energy  $\Delta E_a = 21.1$  kJ/mol derived from the potential energy curve dihedral angle rotation matches well with our experimentally measured value of  $19 - 21$  kJ/mol.

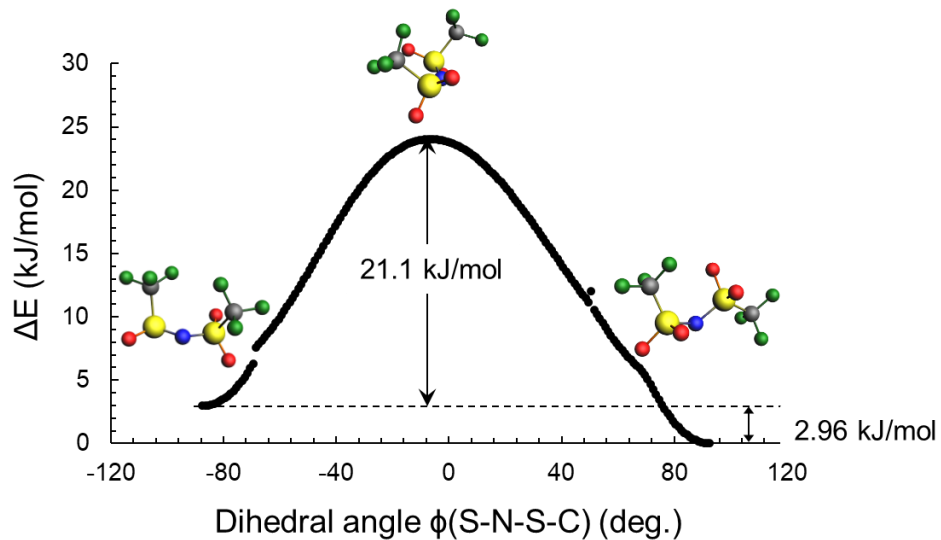


**Figure 7.** Potential energy curve for the pseudo rotation of TFSI by varying  $\phi(\text{S}-\text{N}-\text{S}-\text{C})$  from  $-90^\circ$  to  $90^\circ$ .

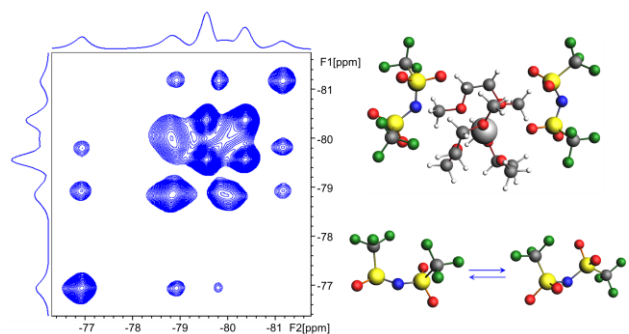
## Conclusion

In the work presented here, we detected distinct TFSI conformal states and associated exchange rates as well as activation energies within the adduct material  $\text{Mg}(\text{TFSI})_2 \cdot \text{DME}$  using  $^{19}\text{F}$  1D and 2D solid-state MAS NMR. The combination of  $^{19}\text{F}$  single-pulse, 2D NOESY and ROESY NMR experiments demonstrate that at  $8\text{ }^\circ\text{C}$ , 45% of adduct TFSI stays in the crystalline region adopting the *trans* conformer, while 55% of the TFSI remains in the disordered region where TFSI experiences conformational exchange between *cis* and *trans* conformations. The *cis-trans* exchange rate is estimated to be  $13.6 - 17.6\text{ s}^{-1}$  at  $8\text{ }^\circ\text{C}$  with  $\Delta H^\ddagger = 19 - 24\text{ kJ/mol}$ , but the rotation of the entire TFSI anion is slower at a rate of  $4.8\text{ s}^{-1}$  at  $8\text{ }^\circ\text{C}$  with a significantly greater  $\Delta H^\ddagger = 98 \pm 10\text{ kJ/mol}$ . As temperature increases, the exchange rates become faster in the disordered region and then in the crystalline area. Concurrently,  $^1\text{H}$  NMR shows that some coordinating DME molecules (with  $\text{Mg}^{2+}$ ) disengage from the first coordinating shell at  $T \geq 52\text{ }^\circ\text{C}$ . On the other hand, as temperature decreases to  $T \leq -1\text{ }^\circ\text{C}$ , TFSI within the crystalline region slowly undergoes conformational change from *trans* to *cis* at a conversion rate of  $1.9 \times 10^{-5}\text{ s}^{-1}$  because the significantly reduced molecular motion of TFSI and DME at a lower temperature prefers the *cis* conformer with a greater dipole moment. Furthermore, DFT calculations provide  $^{19}\text{F}$  chemical shift values that are consistent with our assignment for *cis/trans* conformers, and the activation energy value for *cis-trans* transition (21.1 kJ/mol) is also in good agreement with our experimental result. The combination of  $^{19}\text{F}$  and  $^1\text{H}$  1D and 2D NMR experiments with DFT NMR calculations demonstrated here will be further used to study TFSI conformation, dynamics, and decomposition products within electrode-electrolyte interphases where TFSI molecular motion may lie at the similar time scale as in the adduct material.

## **Acknowledgements**

This work was supported by the Joint Center for Energy Storage Research (JCESR), an Energy Innovation Hub funded by the U.S. Department of Energy, Office of Science, Office of Basic Energy Sciences (BES). A portion of the research was performed using EMSL (grid.436923.9), a DOE Office of Science User Facility sponsored by the Office of Biological and Environmental Research. The EMSL supercomputers (Cascade) was utilized as a resource for computational modeling. PNNL is a multi-program national laboratory operated for the DOE by Battelle Memorial Institute under Contract DE-AC06-76RLO 1830.

**Table of Contents (TOC) image**



## Supporting Information

### Probing Conformational Evolution and Associated Dynamics of Mg(N(SO<sub>2</sub>CF<sub>3</sub>)<sub>2</sub>)<sub>2</sub> · Dimethoxyethane Adduct Using Solid-state <sup>19</sup>F and <sup>1</sup>H NMR

Ying Chen<sup>a</sup>, Nicholas R. Jaegers<sup>a</sup>, Kee Sung Han<sup>a</sup>, Hui Wang<sup>a</sup>, Robert P. Young<sup>a</sup>, Rajeev Surendran Assary<sup>b</sup>, Andrew Lipton<sup>a</sup>, Nancy M. Washton<sup>a</sup>, Jianzhi Hu<sup>a</sup>, Vijayakumar Murugesan<sup>a\*</sup>, Karl T. Mueller<sup>a\*</sup>

a: The Joint Center for Energy Storage Research (JCESR), Pacific Northwest National Laboratory, Richland, WA 99352, USA

b: The Joint Center for Energy Storage Research (JCESR), Argonne National Laboratory, Lemont, IL 60439, USA

\*To whom correspondence should be made

[Vijay@pnnl.gov](mailto:Vijay@pnnl.gov); (509) 371-6540

[Karl.Mueller@pnnl.gov](mailto:Karl.Mueller@pnnl.gov); (509) 371-6550.

**Temperature calibration for fast magic angle spinning:** It has been reported that the sample temperature within a spinning rotor can be significantly different from the probe set temperature, especially at a spinning speed  $> 10$  kHz.<sup>26,27</sup> Since the structure and dynamics of Mg(TFSI)<sub>2</sub>·DME are extremely sensitive to temperature, we calibrated the sample temperature at varying spinning speed using solid lead nitrate Pb(NO<sub>3</sub>)<sub>2</sub>. Figure S1 shows the sample temperature calculated from Pb(NO<sub>3</sub>)<sub>2</sub> chemical shift plotted as a function of rotor spinning speed when the probe temperature is set at 20 °C (A) and the sample temperature as a function of probe set temperature when the spinning speed is set at 24 kHz (B). At a spinning speed of 32 kHz, the sample temperature can reach up to 62 °C with a set temperature at 20 °C. In order to study the materials at a temperature range (-5 – 90 °C) that is relevant to the battery operation conditions, we choose a spinning speed of 24 kHz that is fast enough to remove most chemical shift anisotropy and dipolar interactions in these materials while still staying within the temperature control limits of our instrument (-30 – 80 °C).

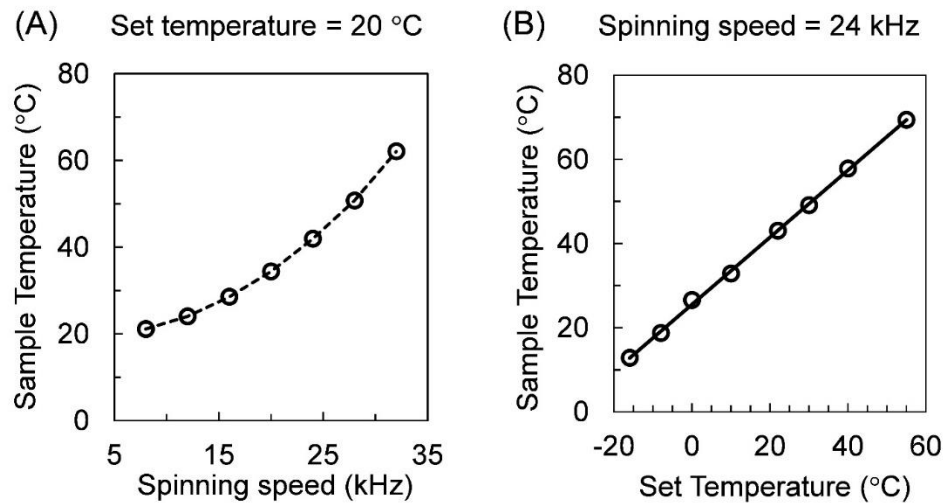


Figure S1. (A) Sample temperature calculated from  $\text{Pb}(\text{NO}_3)_2$  chemical shift plotted as a function of rotor spinning speed when the probe temperature is set at 20 °C. (B) Sample temperature as a function of probe set temperature when the spinning speed is set at 24 kHz.

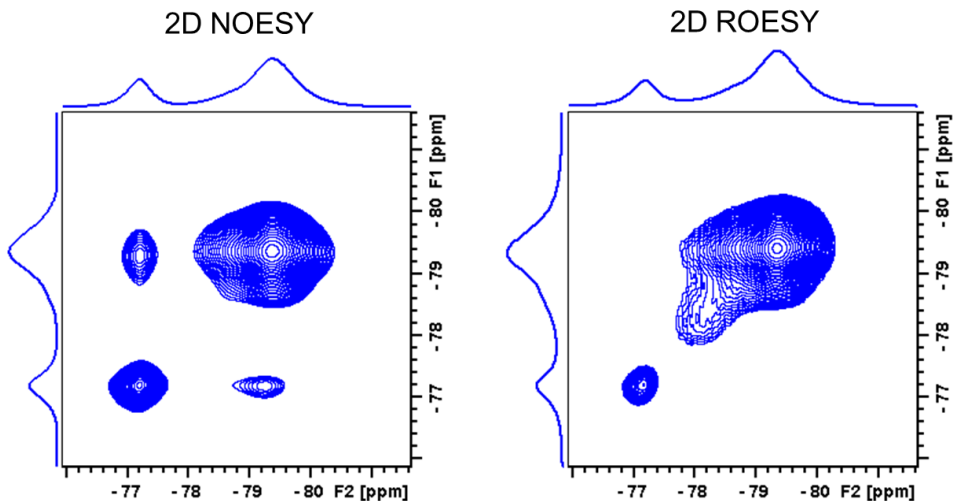


Figure S2.  $^{19}\text{F}$ - $^{19}\text{F}$  2D NOESY (left panel) and ROESY (right panel) spectra of  $\text{Mg}(\text{TFSI})_2$  obtained at 8 °C with a spinning speed of 24 kHz and a mixing time of 50 ms.

The lack of ROESY cross peaks in  $\text{Mg}(\text{TFSI})_2$  suggests that TFSI anions do not experience conformational exchange under the experimental conditions, while the cross peaks shown in NOESY can be explained by spin diffusion between  $^{19}\text{F}$  nuclei in the fluorine-rich hydrophobic layers.

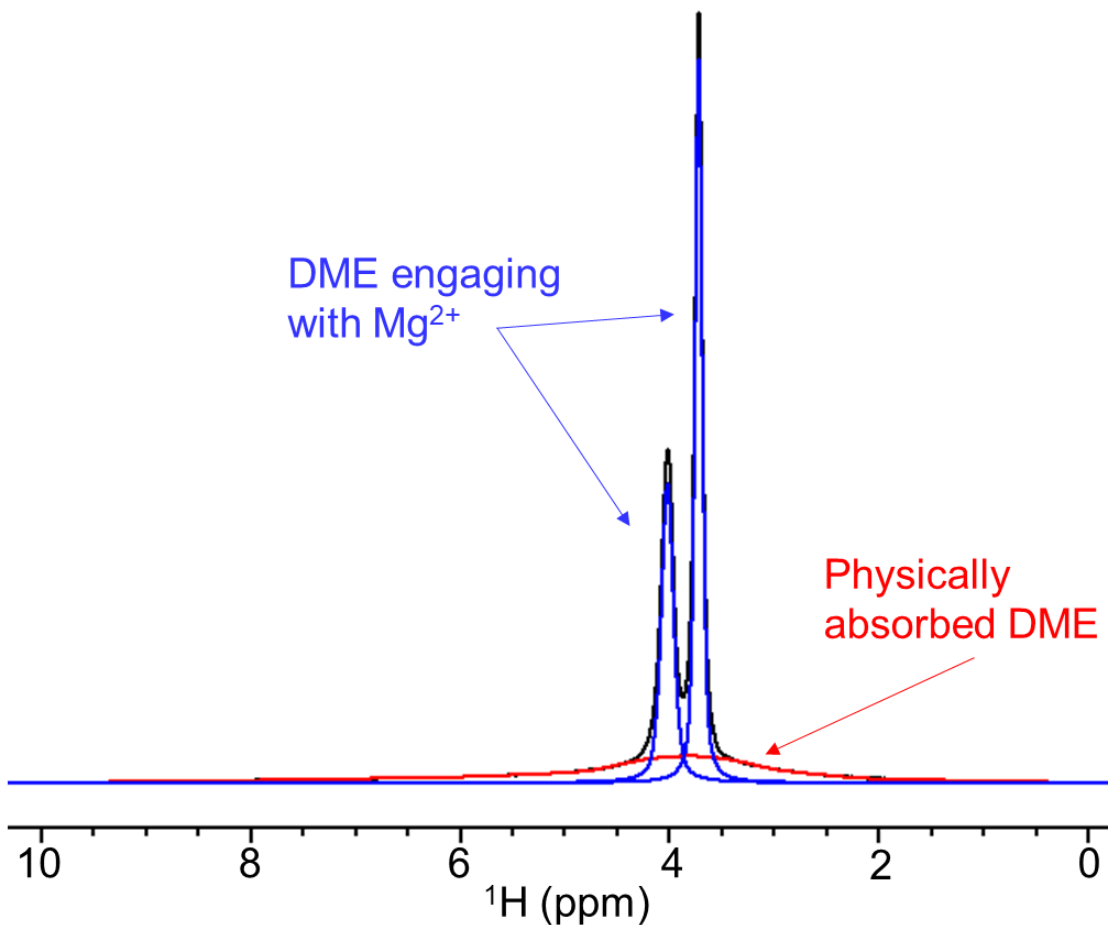


Figure S3.  $^1\text{H}$  MAS NMR of  $\text{Mg}(\text{TFSI})_2\text{-DME}$  collected at 8  $^\circ\text{C}$  with a spinning speed of 24 kHz. The black line is the experimental spectrum, the blue lines are the two  $^1\text{H}$  resonances located at 4.20 and 3.90 ppm resulting from DME molecules engaging with  $\text{Mg}^{2+}$  in the crystalline region, and the red line is the broad peak that arises from physically absorbed DME in the disordered region.

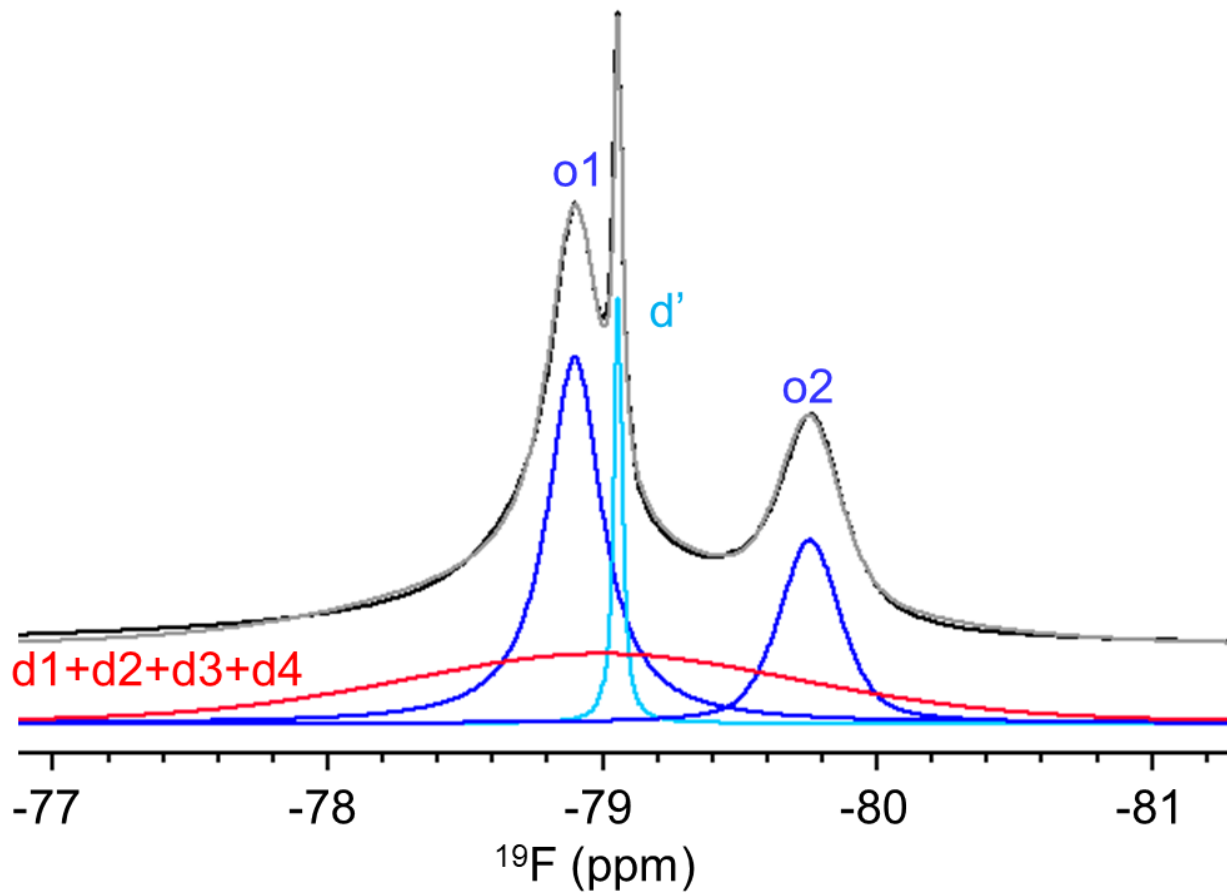


Figure S4.  $^{19}\text{F}$  MAS spectrum of  $\text{Mg}(\text{TFSI})_2\cdot\text{DME}$  collected at  $67\text{ }^\circ\text{C}$  with a spinning speed of 24 kHz. Black line is the experimental spectrum, grey line is the sum of all deconvolution peaks. Red broad peak is from TFSI in disordered regions with fast exchange between d1, d2, d3, and d4 sites, two blue lines O1 and O2 are from TFSI in the crystalline region, and d' is the very fast tumbling TFSI in the disordered region.

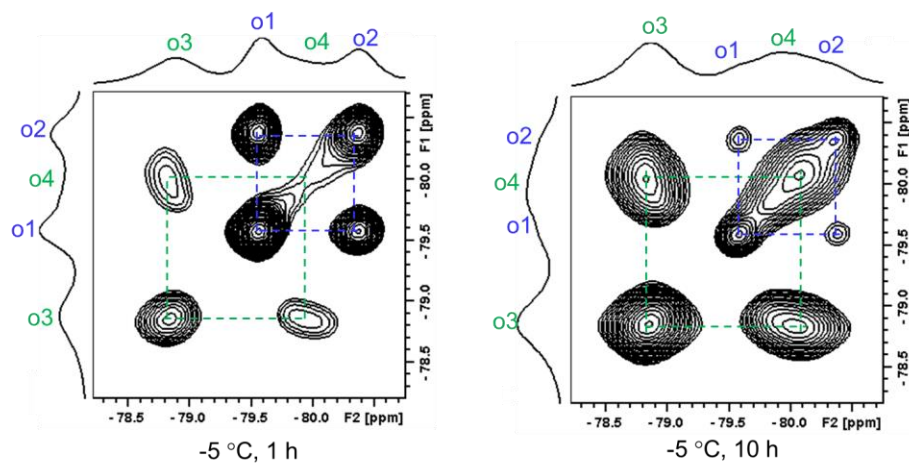
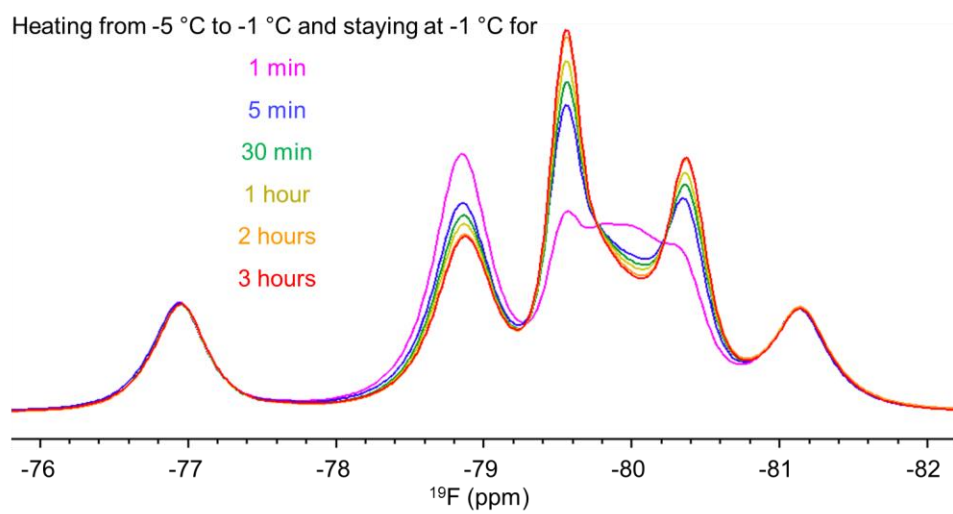
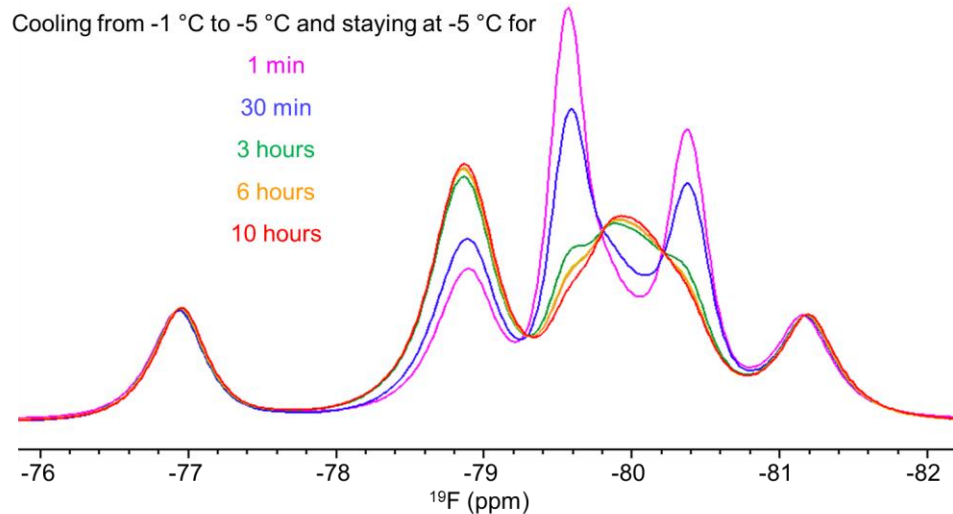


Figure S5.  $^{19}\text{F}$  MAS spectra of  $\text{Mg}(\text{TFSI})_2\cdot\text{DME}$  when cooling from -1 °C to -5 °C until equilibrium (upper panel), and heating from -5 °C to -1 °C and held at -1 °C until equilibrium (lower panel); as well as the 2D NOESY spectra collected at -5 °C after the temperature stabilizing for 1 hour and 10 hours.

When cooling the material down from 82 °C to 38 °C and finally 8 °C for approximately 3 hours at each temperature until no change in  $^{19}\text{F}$  and  $^1\text{H}$  NMR is observed, compared with the previous spectra at 38 °C and 8 °C, it is clear that the heating process at 82 °C is not completely reversible, a few percent of DME in the second coordination shell and fast tumbling TFSI in the disordered region do not return to their original state. Also, both  $\text{d}^\circ$  and  $\text{CH}_2^\circ/\text{CH}_3^\circ$  peaks decreased its intensity simultaneously as the decrease in temperature which suggests that the thermally activated fast molecular motion of TFSI in the disordered region and DME molecules became slower at the lower temperature.

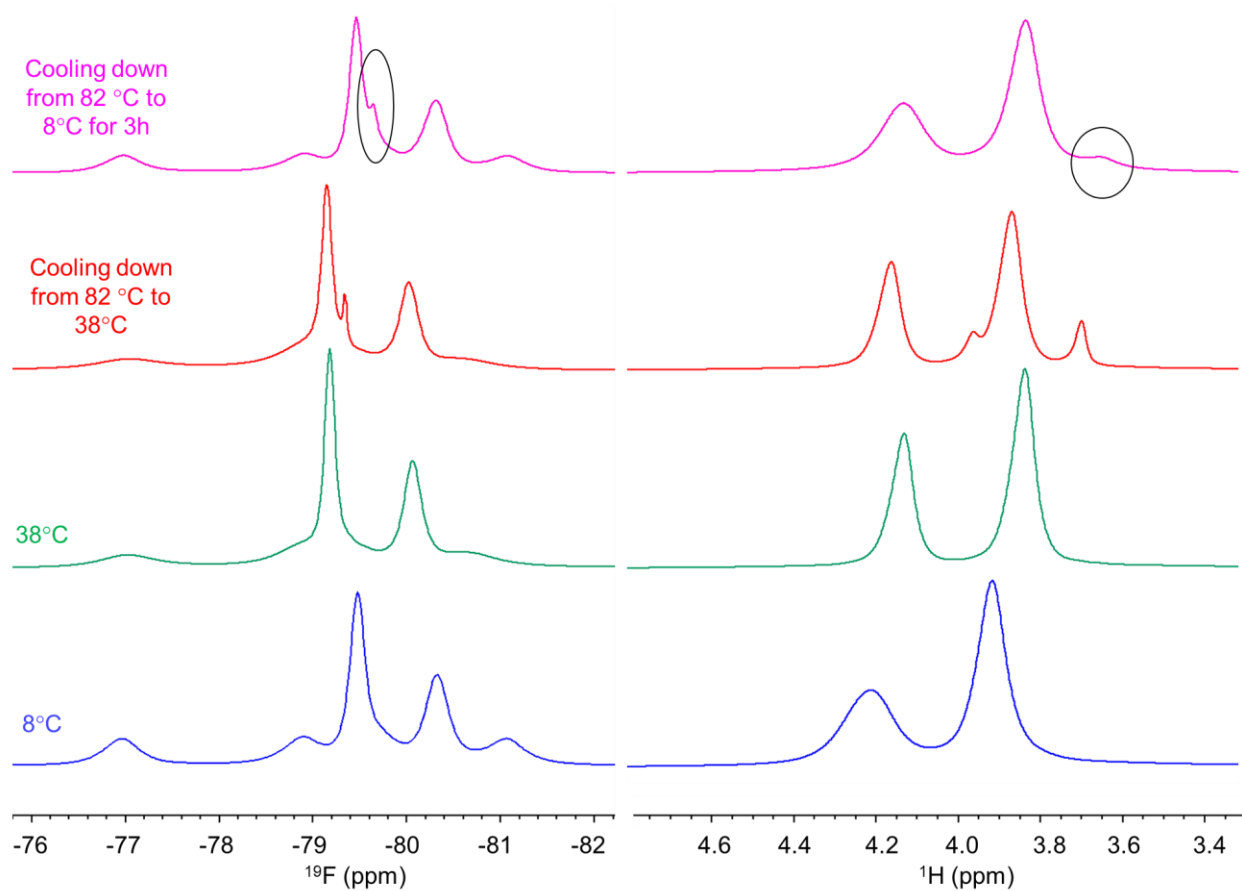
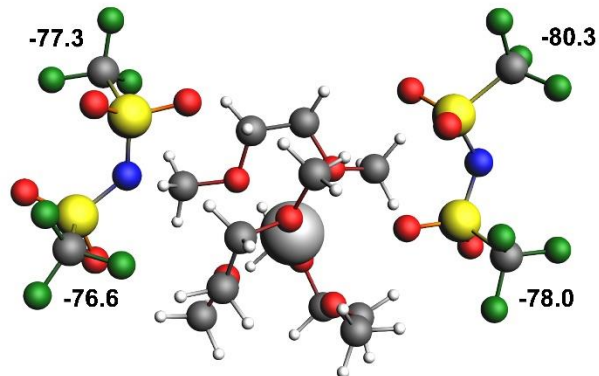
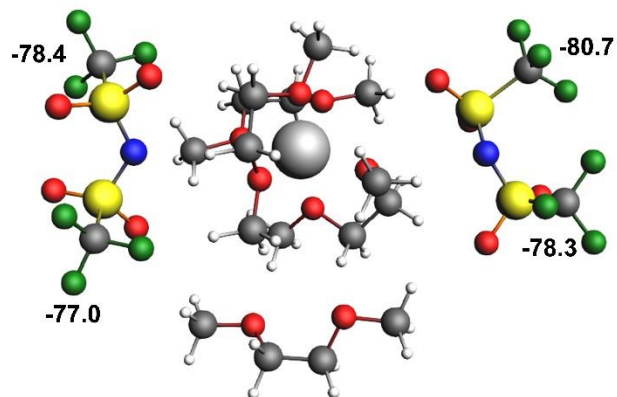


Figure S6.  $^{19}\text{F}$  and  $^1\text{H}$  MAS spectrum of  $\text{Mg}(\text{TFSI})_2\cdot\text{DME}$  at  $8\text{ }^\circ\text{C}$  (blue) and  $38\text{ }^\circ\text{C}$  (green) and cooling down from  $82\text{ }^\circ\text{C}$  back to  $38\text{ }^\circ\text{C}$  (red) and  $8\text{ }^\circ\text{C}$  (pink), with a spinning speed of 24 kHz.

$\text{Mg}(\text{DME})_3(\text{TFSI})_2$



$\text{Mg}(\text{DME})_3(\text{TFSI})_2(\text{DME})$



$\text{Mg}(\text{DME})_3(\text{TFSI})_2(\text{DME})_4$

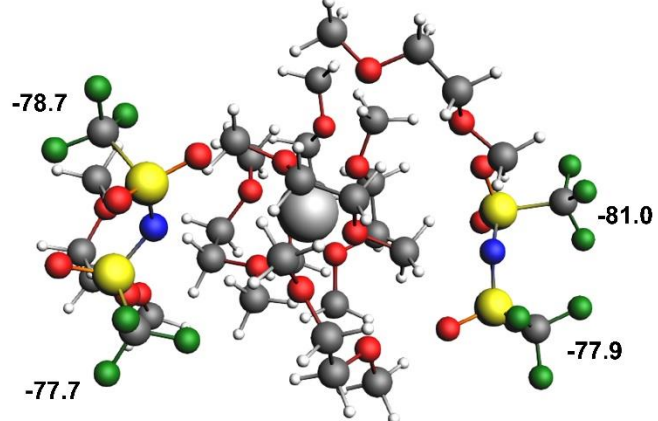


Figure S7. Chemical shift values of  $\text{Mg}(\text{TFSI})_2\cdot\text{DME}$  clusters calculated using TZ2PJ basis in ADF.

## Reference

1. Hallett, J. P.; Welton, T., Room-Temperature Ionic Liquids: Solvents for Synthesis and Catalysis. 2. *Chemical Reviews* **2011**, *111* (5), 3508-3576.
2. Lewandowski, A.; Świderska-Mocek, A., Ionic liquids as electrolytes for Li-ion batteries—An overview of electrochemical studies. *Journal of Power Sources* **2009**, *194* (2), 601-609.
3. Best, A. S.; Bhatt, A. I.; Hollenkamp, A. F., Ionic Liquids with the Bis(fluorosulfonyl)imide Anion: Electrochemical Properties and Applications in Battery Technology. *Journal of The Electrochemical Society* **2010**, *157* (8), A903-A911.
4. Ha, S.-Y.; Lee, Y.-W.; Woo, S. W.; Koo, B.; Kim, J.-S.; Cho, J.; Lee, K. T.; Choi, N.-S., Magnesium(II) Bis(trifluoromethane sulfonyl) Imide-Based Electrolytes with Wide Electrochemical Windows for Rechargeable Magnesium Batteries. *ACS Applied Materials & Interfaces* **2014**, *6* (6), 4063-4073.
5. Canepa, P.; Sai Gautam, G.; Hannah, D. C.; Malik, R.; Liu, M.; Gallagher, K. G.; Persson, K. A.; Ceder, G., Odyssey of Multivalent Cathode Materials: Open Questions and Future Challenges. *Chemical Reviews* **2017**, *117* (5), 4287-4341.
6. Lapidus, S. H.; Rajput, N. N.; Qu, X.; Chapman, K. W.; Persson, K. A.; Chupas, P. J., Solvation structure and energetics of electrolytes for multivalent energy storage. *Physical Chemistry Chemical Physics* **2014**, *16* (40), 21941-21945.
7. Johansson, P.; Gejji, S. P.; Tegenfeldt, J.; Lindgren, J., The imide ion: potential energy surface and geometries. *Electrochimica Acta* **1998**, *43* (10), 1375-1379.
8. Watkins, T.; Buttry, D. A., Determination of Mg<sup>2+</sup> Speciation in a TFSI-Based Ionic Liquid With and Without Chelating Ethers Using Raman Spectroscopy. *The Journal of Physical Chemistry B* **2015**, *119* (23), 7003-7014.
9. Salama, M.; Shterenberg, I.; Gizbar, H.; Eliaz, N. N.; Kosa, M.; Keinan-Adamsky, K.; Afri, M.; Shimon, L. J. W.; Gottlieb, H. E.; Major, D. T.; Gofer, Y.; Aurbach, D., Unique Behavior of Dimethoxyethane (DME)/Mg(N(SO<sub>2</sub>CF<sub>3</sub>)<sub>2</sub>)<sub>2</sub> Solutions. *The Journal of Physical Chemistry C* **2016**, *120* (35), 19586-19594.
10. Shterenberg, I.; Salama, M.; Yoo, H. D.; Gofer, Y.; Park, J.-B.; Sun, Y.-K.; Aurbach, D., Evaluation of (CF<sub>3</sub>SO<sub>2</sub>)<sub>2</sub>N<sup>-</sup> (TFSI) Based Electrolyte Solutions for Mg Batteries. *Journal of The Electrochemical Society* **2015**, *162* (13), A7118-A7128.
11. Rajput, N. N.; Qu, X.; Sa, N.; Burrell, A. K.; Persson, K. A., The Coupling between Stability and Ion Pair Formation in Magnesium Electrolytes from First-Principles Quantum Mechanics and Classical Molecular Dynamics. *Journal of the American Chemical Society* **2015**, *137* (9), 3411-3420.
12. Herstedt, M.; Smirnov, M.; Johansson, P.; Chami, M.; Grondin, J.; Servant, L.; Lassègues, J. C., Spectroscopic characterization of the conformational states of the bis(trifluoromethanesulfonyl)imide anion (TFSI<sup>-</sup>). *Journal of Raman Spectroscopy* **2005**, *36* (8), 762-770.
13. Fujii, K.; Fujimori, T.; Takamuku, T.; Kanzaki, R.; Umebayashi, Y.; Ishiguro, S.-i., Conformational Equilibrium of Bis(trifluoromethanesulfonyl) Imide Anion of a Room-Temperature Ionic Liquid: Raman Spectroscopic Study and DFT Calculations. *The Journal of Physical Chemistry B* **2006**, *110* (16), 8179-8183.
14. Duluard, S.; Grondin, J.; Bruneel, J.-L.; Pianet, I.; Grélard, A.; Campet, G.; Delville, M.-H.; Lassègues, J.-C., Lithium solvation and diffusion in the 1-butyl-3-methylimidazolium bis(trifluoromethanesulfonyl)imide ionic liquid. *Journal of Raman Spectroscopy* **2008**, *39* (5), 627-632.
15. Lassègues, J.-C.; Grondin, J.; Aupetit, C.; Johansson, P., Spectroscopic Identification of the Lithium Ion Transporting Species in LiTFSI-Doped Ionic Liquids. *The Journal of Physical Chemistry A* **2009**, *113* (1), 305-314.
16. Veryasov, G.; Harinaga, U.; Matsumoto, K.; Hagiwara, R., Crystallographic Insight into the Mg<sup>2+</sup> Coordination Mode and N(SO<sub>2</sub>CF<sub>3</sub>)<sub>2</sub><sup>-</sup> Anion Conformation in Mg[N(SO<sub>2</sub>CF<sub>3</sub>)<sub>2</sub>]<sub>2</sub> and Its Adducts. *European Journal of Inorganic Chemistry* **2017**, *2017* (7), 1087-1099.

17. Nowinski, J. L.; Lightfoot, P.; Bruce, P. G., Structure of LiN(CF<sub>3</sub>SO<sub>2</sub>)<sub>2</sub>, a novel salt for electrochemistry. *Journal of Materials Chemistry* **1994**, *4* (10), 1579-1580.

18. Xue, L.; Padgett, C. W.; DesMarteau, D. D.; Pennington, W. T., Synthesis and structures of alkali metal salts of bis[(trifluoromethyl)sulfonyl]imide. *Solid State Sciences* **2002**, *4* (11), 1535-1545.

19. Matsumoto, K.; Matsui, T.; Nohira, T.; Hagiwara, R., Crystal structure of Na[N(SO<sub>2</sub>CF<sub>3</sub>)<sub>2</sub>] and coordination environment of alkali metal cation in the M[N(SO<sub>2</sub>CF<sub>3</sub>)<sub>2</sub>] (M+=Li<sup>+</sup>, Na<sup>+</sup>, K<sup>+</sup>, and Cs<sup>+</sup>) structures. *Journal of Fluorine Chemistry* **2015**, *174*, 42-48.

20. Salama, M.; Shterenberg, I.; J.W. Shimon, L.; Keinan-Adamsky, K.; Afri, M.; Gofer, Y.; Aurbach, D., Structural Analysis of Magnesium Chloride Complexes in Dimethoxyethane Solutions in the Context of Mg Batteries Research. *The Journal of Physical Chemistry C* **2017**, *121* (45), 24909-24918.

21. R., D. J. W., *Guide to Fluorine NMR for Organic Chemists*. John Wiley & Sons, Inc.: Hoboken, New Jersey, 2016.

22. Hayamizu, K.; Tsuzuki, S.; Seki, S., Molecular Motions and Ion Diffusions of the Room-Temperature Ionic Liquid 1,2-Dimethyl-3-propylimidazolium Bis(trifluoromethylsulfonyl)amide (DMPImTFSA) Studied by <sup>1</sup>H, <sup>13</sup>C, and <sup>19</sup>F NMR. *The Journal of Physical Chemistry A* **2008**, *112* (47), 12027-12036.

23. Kunze, M.; Montanino, M.; Appetecchi, G. B.; Jeong, S.; Schönhoff, M.; Winter, M.; Passerini, S., Melting Behavior and Ionic Conductivity in Hydrophobic Ionic Liquids. *The Journal of Physical Chemistry A* **2010**, *114* (4), 1776-1782.

24. Hayamizu, K.; Tsuzuki, S.; Seki, S.; Umebayashi, Y., Multinuclear NMR Studies on Translational and Rotational Motion for Two Ionic Liquids Composed of BF<sub>4</sub> Anion. *The Journal of Physical Chemistry B* **2012**, *116* (36), 11284-11291.

25. D'Agostino, C.; Mantle, M. D.; Mullan, C. L.; Hardacre, C.; Gladden, L. F., Diffusion, Ion Pairing and Aggregation in 1-Ethyl-3-Methylimidazolium-Based Ionic Liquids Studied by <sup>1</sup>H and <sup>19</sup>F PFG NMR: Effect of Temperature, Anion and Glucose Dissolution. *ChemPhysChem* **2018**, *19* (9), 1081-1088.

26. Brus, J., Heating of samples induced by fast magic-angle spinning. *Solid State Nuclear Magnetic Resonance* **2000**, *16* (3), 151-160.

27. Guan, X.; Stark, R. E., A general protocol for temperature calibration of MAS NMR probes at arbitrary spinning speeds. *Solid State Nuclear Magnetic Resonance* **2010**, *38* (2), 74-76.

28. Macura, S.; Ernst, R. R., Elucidation of cross relaxation in liquids by two-dimensional N.M.R. spectroscopy. *Molecular Physics* **1980**, *41* (1), 95-117.

29. Perrin, C. L.; Gipe, R. K., Multisite kinetics by quantitative two-dimensional NMR. *Journal of the American Chemical Society* **1984**, *106* (14), 4036-4038.

30. Willem, R., 2D NMR applied to dynamic stereochemical problems. *Progress in Nuclear Magnetic Resonance Spectroscopy* **1988**, *20* (1), 1-94.

31. te Velde, G.; Bickelhaupt, F. M.; Baerends, E. J.; Fonseca Guerra, C.; van Gisbergen, S. J. A.; Snijders, J. G.; Ziegler, T., Chemistry with ADF. *Journal of Computational Chemistry* **2001**, *22* (9), 931-967.

32. Fonseca Guerra, C.; Snijders, G. J.; te Velde, G.; Baerends, J. E., Towards an order-N DFT method. *Theoretical Chemistry Accounts* **99** (6), 391-403.

33. ADF2014 SCM, Vrije Universiteit, Amsterdam, The Netherlands, <http://www.scm.com>.

34. Perdew, J. P.; Burke, K.; Ernzerhof, M., Generalized gradient approximation made simple. *Physical Review Letters* **1996**, *77* (18), 3865-3868.

35. Grimme, S.; Ehrlich, S.; Goerigk, L., Effect of the Damping Function in Dispersion Corrected Density Functional Theory. *Journal of Computational Chemistry* **2011**, *32* (7), 1456-1465.

36. Van Lenthe, E.; Baerends, E. J., Optimized Slater-type basis sets for the elements 1–118. *Journal of Computational Chemistry* **2003**, *24* (9), 1142-1156.

37. Schreckenbach, G.; Ziegler, T., Calculation of Nmr Shielding Tensors Using Gauge-Including Atomic Orbitals and Modern Density-Functional Theory. *J Phys Chem-Us* **1995**, *99* (2), 606-611.

38. Schreckenbach, G.; Ziegler, T., The calculation of NMR shielding tensors based on density functional theory and the frozen-core approximation. *International Journal of Quantum Chemistry* **1996**, *60* (3), 753-766.

39. Schreckenbach, G.; Ziegler, T., Calculation of NMR shielding tensors based on density functional theory and a scalar relativistic Pauli-type Hamiltonian. The application to transition metal complexes. *International Journal of Quantum Chemistry* **1997**, *61* (6), 899-918.

40. Henderson, W. A.; Seo, D. M.; Zhou, Q.; Boyle, P. D.; Shin, J.-H.; De Long, H. C.; Trulove, P. C.; Passerini, S., An Alternative Ionic Conductivity Mechanism for Plastic Crystalline Salt–Lithium Salt Electrolyte Mixtures. *Advanced Energy Materials* **2012**, *2* (11), 1343-1350.

41. Xue, L.; DesMarteau, D. D.; Pennington, W. T., Synthesis and structures of alkaline earth metal salts of bis[(trifluoromethyl)sulfonyl]imide. *Solid State Sciences* **2005**, *7* (3), 311-318.

42. Gupta, A.; Murugan, R.; Paranthaman, M. P.; Bi, Z.; Bridges, C. A.; Nakanishi, M.; Sokolov, A. P.; Han, K. S.; Hagaman, E. W.; Xie, H.; Mullins, C. B.; Goodenough, J. B., Optimum lithium-ion conductivity in cubic  $\text{Li}_{7-x}\text{La}_3\text{Hf}_2-x\text{Ta}_x\text{O}_{12}$ . *Journal of Power Sources* **2012**, *209*, 184-188.

43. Eyring, H., The Activated Complex in Chemical Reactions. *The Journal of Chemical Physics* **1935**, *3* (2), 107-115.

44. Laidler, K. J.; King, M. C., Development of transition-state theory. *The Journal of Physical Chemistry* **1983**, *87* (15), 2657-2664.